Catarina Isabel de Sousa Lopes

Bachelor Degree in Human Biology

Using AFM to study erythrocytes' biophysical properties on Stroke and Amyotrophic Lateral Sclerosis

Dissertation to obtain the Master of Science Degree in Molecular Genetic and Biomedicine

Supervisor: Professora Doutora Filomena A. Carvalho

Júri:
Presidente: Prof. Doutora Margarida Castro Caldas Braga, FCT-UNL
Arguente: Prof. Doutora Ana Cecília Roque, FCT-UNL
Orientadora: Prof. Doutora Filomena A. Carvalho, IMM

FACULDADE DE CIÊNCIAS E TECNOLOGIA
UNIVERSIDADE NOVA DE LISBOA

September 2016

Using AFM to study erythrocytes' biophysical properties on Stroke and Amyotrophic Lateral Sclerosis

Catarina Isabel de Sousa Lopes

2016

Catarina Isabel de Sousa Lopes

Bachelor degree in Human Biology

Using AFM to study erythrocytes' biophysical properties on Stroke and Amyotrophic Lateral Sclerosis

Dissertation to obtain the Master of Science Degree in Molecular Genetic and Biomedicine

Supervisor: Professora Doutora Filomena A. Carvalho

FACULDADE DE CIÊNCIAS E TECNOLOGIA
UNIVERSIDADE NOVA DE LISBOA

September 2016

Using AFM to study erythrocytes' biophysical properties on Stroke and Amyotrophic Lateral Sclerosis

Acknowledgments

Firstly, I would like to thank Prof. Nuno C. Santos, for kindly receiving me in his research group (Biomembranes Unit), and for the opportunity to develop my project thesis. I am very grateful for all excellent working conditions that he provided in our lab, which improved my scientific education. I also thank him for believing in my capabilities to develop this project.

Secondly, I am also grateful to my awesome supervisor, Prof. Filomena A. Carvalho, with whom I worked every day, during the development of my thesis. I would like to thank for her attention and patience with me, for teaching and showing me how to do science, and for believing in my capabilities.

I also would like to thank Prof. Mamede de Carvalho and Ana Catarina Pronto Laborinho for the opportunity to work in Amyotrophic Lateral Sclerosis disease, and for the great discussions of the results included on this thesis.

I am grateful to Ana Filipa Guedes, my partner during this project, who helped me along this year, for her attention and time spent explaining some methodologies used on this project. I would also like thank Teresa Freitas, for her friendship and help during this thesis. To all the researchers of the Biomembranes Unit, especially, to Patrícia Silva, I am grateful for her friendship and for every moments in the laboratory and snapchats and dramas along the development of the thesis.

To my dear friends Filipa Gonçalves, Margarida L. Ferreira, Ana Pinto, Catarina Morgado, Mafalda Azevedo Gomes, for their friendship, adventures, patience, positive support and relaxing moments, specially during this year.

To all my friends and every people that make me be a better person.

I would like to thank all my family (grandmothers, uncle and cousins), for their positive support along this year.

Finally, a very special thanks to my parents, João and Maria, and my sister, Sara, for all their love and encouragement. Without them it will be impossible to finish this thesis.

Thank you very much to all!!

Abstract

Stroke is the most common cause of death worldwide. It is associated with high fibrinogen levels in plasma. Fibrinogen promotes clot formation, which in some situations can promote venous thromboembolism. Amyotrophic Lateral Sclerosis (ALS) is a devastating and fatal neurodegenerative disease, leading to severe respiratory insufficiency and hypoxia.

The main goals of this study were: (i) to study the influence of fibrinogen on erythrocytes adhesion in stroke patients; and, (ii) to evaluate morphological and elasticity changes on erythrocytes from ALS patients.

Human blood samples from stroke and ALS patients were analysed and compared with healthy donors (control).

Samples were analysed by Atomic Force Microscopy (AFM) and through haemorheological parameters. AFM was used to measure fibrinogen-erythrocyte and erythrocyte-erythrocyte interactions, as well as erythrocyte stiffness and morphology. Erythrocyte membrane fluidity and zeta-potential were also assessed on ALS.

Erythrocytes from stroke patients are less deformable and have more propensity to aggregate. Fibrinogen-erythrocytes interactions on stroke are stronger than for the control group. They also have an increased concentration of γ´ fibrinogen variant. These changes could be associated with high risk of cardiovascular events and a worst prognostic of the disease.

Erythrocytes from ALS patients are more capable to deform and present morphological changes. Changes in erythrocytes physical-chemical and electrical properties and on their membrane organization were also observed.

These findings could help to consider the fibrinogen-erythrocyte binding as a new cardiovascular risk factor for stroke disease. Understanding the role of fibrinogen on erythrocyte aggregation may be relevant for potential future drug interventions to reduce aggregation and enhance microcirculatory flow conditions. Fibrinogen in ALS disease could promote venous thrombotic events. In the future, finding a molecular biomarker of early respiratory dysfunction in ALS disease that could comprise prognostic value will be essential.

Keywords: Stroke; Amyotrophic Lateral Sclerosis (ALS); Atomic Force Microscopy (AFM); Erythrocyte; Fibrinogen.

Resumo

O acidente vascular cerebral (AVC) é a maior causa de morte mundial. A ele estão associados elevados níveis de fibrinogénio plasmáticos. O fibrinogénio promove o processo de coagulação sanguínea, podendo nalgumas situações conduzir a tromboembolismo venoso. A Esclerose Lateral Amiotrófica (ELA) é uma doença neurodegenerativa fatal, podendo conduzir a insuficiência respiratória e hipóxia.

Os principais objetivos deste estudo foram: (i) estudar a influência do fibrinogénio na adesão eritrocitária em doentes com AVC; (ii) avaliar alterações morfológicas e de elasticidade nos eritrócitos de doentes com ELA.

Amostras de sangue humano de doentes com AVC e ELA foram comparadas com amostras de dadores saudáveis (controlo). Estas foram analisadas por microscopia de força atómica (AFM) e por parâmetros hemorreológicos. Por AFM estudaram-se interações fibrinogénio-eritrócito e adesão eritrócito-eritrócito, assim como a elasticidade e morfologia eritrocitárias. A fluidez da membrana e o seu potencial zeta foram também avaliados na ELA.

Os eritrócitos de doentes com AVC são menos deformáveis e têm mais propensão para agregar. As interações fibrinogénio-eritrócito são mais fortes que no grupo controlo. Estes doentes têm também um aumento da concentração de fibrinogénio γ'. Estas alterações poderão estar associadas ao elevado risco de eventos cardiovasculares e ao mau prognóstico da doença.

Os eritrócitos de ELA são mais deformáveis e têm alterações morfológicas. Alterações físico-químicas e das propriedades elétricas dos eritrócitos, bem como da sua membrana foram também observadas.

Estes resultados permitem identificar a interação fibrinogénio-eritrócito como novo fator de risco cardiovascular em AVC. O papel do fibrinogénio na agregação eritrocitária poderá ser relevante na futura utilização de fármacos que reduzam a agregação e melhorem a microcirculação. Em ELA, o fibrinogénio poderá promover tromboembolismo venoso. O desenvolvimento de um biomarcador molecular precoce de disfunção respiratória na ELA com valor no prognóstico da doença é assim essencial.

Palavras-Chave: Acidente Vascular Cerebral (AVC); Esclerose Lateral Amiotrófica (ELA); Microscópio de Força Atómica; Eritrócito; Fibrinogénio.

Table of Contents

List of Figures

List of Tables

Abbreviations

AFM
Atomic Force Microscopy
ALS
Amyotrophic Lateral Sclerosis
AMI
Acute Myocardial Infarction
APTES
3-aminopropyl-triethoxysilane
BIOTIN-BSA
Biotinylated Bovine Serum Albumin
BSGC
Buffered Saline Glucose-Citrate
CHD
Coronary Heart Disease
CV
Cardiovascular
CVD
Cardiovascular Disease
DMSO
Dimethyl sulphoxide
ECM
Extracellular Matrix
ELISA
Enzyme-Linked Immunosorbent Assay
FALS
Familial Amyotrophic Lateral Sclerosis
GP
Generalized Polarization
JC
Junctional Complex
LAURDAN
2-dimethylamino-6-lauroylnaphthalene
MND
Motor Neuron Disease
PBS
Phosphate Buffered Saline
RBC
Red Blood Cell
SEM
Standard Error of the Mean
SALS
Sporadic Amyotrophic Lateral Sclerosis
SCFS
Single-Cell Force Spectroscopy
SMFS
Single-Molecule Force Spectroscopy
SOD
Super Oxide Dismutase
TF
Tissue Factor
VTE
Venous Thromboembolism

I) General Introduction

1) Stroke

The cardiovascular diseases (CVD) are the most common cause of death in the world. In 2012, it was estimated that 17.5 million people died from CVD, from which an estimated 7.4 million deaths were due to coronary heart disease and 6.7 million were due to stroke (World Health Organization, 2016). Coronary heart disease (CHD) and stroke are prevalent in the world, and 35%–65% of all deaths can be traced to CVD (*vd.* Figure I.1). Typically, the rate of CHD deaths exceeds that of stroke by a ratio from 2:1 to 3:1. During this period, average life expectancy surpasses 50 years. Roughly, 35% of the world's population falls into this category (Longo *et al.*, 2012).

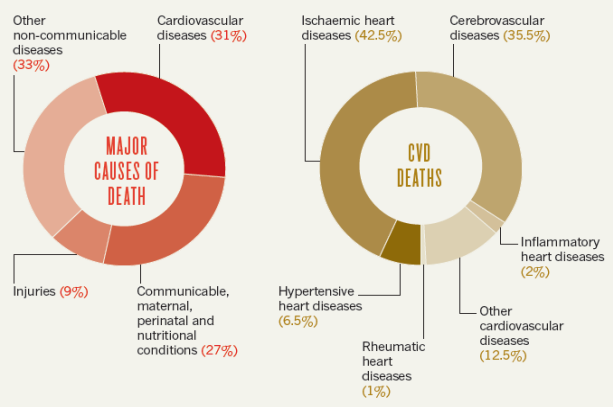

Figure I.1 - Cardiovascular diseases are the main cause of death in the world (31%). The ischaemic heart diseases and the cerebrovascular diseases promote the major part of the CVD deaths. Adapted from (Cannon, 2013)**.**

In Portugal, cardiovascular diseases are also the leading cause of death. In 2012, 32,859 people died from CVD; from those, 14,393 were male and 18,466 female (Sociedade Portuguesa de Cardiologia, 2015).

By 2030, when the world population is expected to reach 8.2 billion, 33% of all deaths are expected to be of CVD (*v.d.* Figure I.2). Also, it is expected that 14.9% of deaths which will occur in men and 13.1% of deaths occur in women will be due to CHD. Stroke is being responsible for 10.4% of all male deaths and 11.8% of all female deaths (Longo *et al.*, 2012).

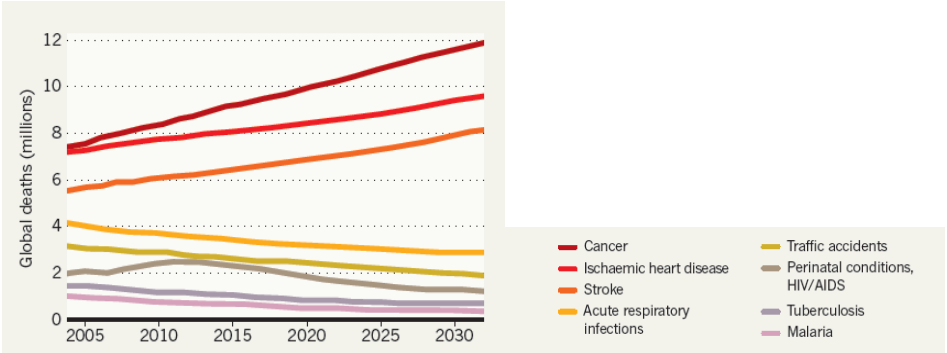

Figure I.2 - By 2030, it is expected that cancer, ischaemic heart disease and stroke will be responsible for an increase of deaths in the world. Adapted from (Cannon, 2013)**.**

The development of a clot in the coronary or cerebral circulation is the cause of an acute myocardial infarction or ischaemic stroke, respectively (Jackson, 2011). Acute myocardial infarction (AMI) and stroke are the most frequent cardiovascular diseases. In real life, stroke does not always have an announcement. It can be silence and quick. Acute events are mainly caused by a blockage of blood circulation that prevents blood from flowing to the heart or brain. This process is mainly due to atherosclerosis. Atherosclerosis happens when coronary arteries, which supply the heart with blood, slowly become thicker and harder from a build-up of fat, cholesterol and other substances, forming an atherosclerotic plaque. If an atherosclerotic plaque ruptures, a blood clot can be formed, and it can travel through the bloodstream, where it can lodge on the artery of the brain, blocking the flow of the oxygen-rich blood. When the blood flow is blocked, the supply of oxygen does not reach part of brain cells and these are damaged or die (Sociedade Portuguesa de Cardiologia, 2015).

Stroke can also be caused by bleeding from a blood vessel in the brain or from blood clots (World Health Organization, 2016). As, it can be seen in Figure I.3, stroke is caused by the disruption of the blood supply to the brain. This may result from either blockage (ischaemic stroke) or rupture of a blood vessel (haemorrhagic stroke) (World Health Organization, 2002).

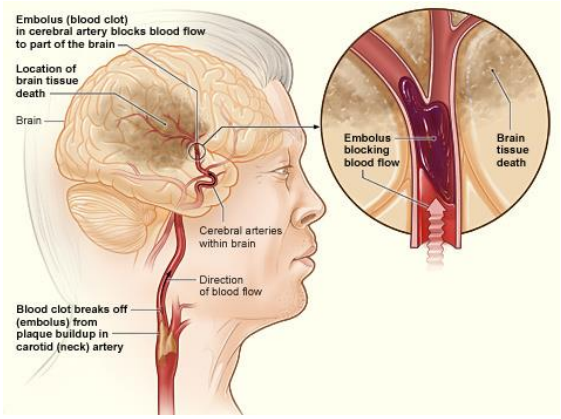

Figure I.3 - Process of a blood clot blocking the blood flow, in the brain artery. When this process occurs, blood flow is blocked, promoting a stroke.
Figure from (http://www.ncbi.nlm.nih.gov/pubmedhealth/PMH0063013/bin/stroke_ischemic.jpg).

1.1) Cardiovascular Risk Factors

The evaluation of novel risk factors can help to identify individuals at higher cardiovascular risk. The prevention of CVD focuses on identifying and managing risk factors, both on the entire population and at individual levels through primordial, primary and secondary prevention. Other causes of CVD are usually the presence of a combination of risk factors, such as unhealthy diet, obesity, physical inactivity, tobacco and alcohol habits. These CV risk factors may lead to other clinical complications, such as hypertension, diabetes mellitus and hyperlipidaemia (Sociedade Portuguesa de Cardiologia, 2015). At the individual level, for the prevention of the first cases of cardiovascular disease, individual

health-care intervention needs to be targeted to those at high cardiovascular risk and high risk factor levels. For the secondary prevention of cardiovascular diseases, medication becomes necessary.

Studies concerning high levels of fibrinogen in blood plasma have associated it with a wide variety of thrombotic diseases, such as stroke. Fibrinogen has been identified as a major independent risk factor for cardiovascular disease (De Oliveira *et al.*, 2012). High fibrinogen levels promote fibrin formation and it is a major contributor to plasma viscosity (Stec *et al.*, 2000). Increased levels of plasma fibrinogen result in changes in blood rheological properties, and these alterations exacerbate the complications in peripheral blood circulation during cardiovascular pathologies. Erythrocyte aggregation is also important, together with fibrinogen and lipids concentration on plasma to understand the risk of primary and secondary cardiovascular events. The interaction between fibrinogen and erythrocytes could be an important indicator of a high cardiovascular risk.

2) Erythrocytes

Erythrocytes, or red blood cells (RBC), are the most abundant cell type in blood. They are flexible, biconcave, enucleate cells derived from bone marrow. Erythrocytes circulate at $4.2\text{-}6.1\times10^9$ cells/mL in humans, having men slightly higher values than women. Erythrocytes are highly specialized cells that carry oxygen from the lungs to the body cells and tissues to the lungs via its haemoglobin-rich cytoplasm (Baskurt & Meiselman, 2003; Dzierzak & Philipsen, 2013; Aleman *et al.*, 2014). Human erythrocytes have an *in vivo* life span of approximately 120 days and they are selectively removed from circulation via phagocytosis. During its life span, the erythrocyte undergoes progressive physical and chemical changes, such as the decrease on cell volume with cell aging. This is presumably due to the loss of potassium and the loss of membrane patches by microvesiculation, resulting in an increase on cell density (Carvalho *et al.*, 2011).

Usually, mature erythrocytes are biconcave disks, with about 8 μm in diameter, however erythrocytes can measure between 6.6 to 7.5 μm. Healthy erythrocytes have a thickness of 2 μm, surface area of 135 μm^2 and volume of 90 fL. They are composed by haemoglobin (32%), water (65%), and membrane tissue (3%) (Yurkin *et al.*, 2005). The erythrocyte membrane is composed of a lipid bilayer, transmembrane proteins, and a filamentous meshwork of proteins that forms a membrane skeleton along the entire cytoplasmic surface of the membrane, as it can be seen in Figure I.4. The erythrocyte membrane skeleton has spectrin as its most abundant protein, which forms long, flexible heterodimers through the lateral association between chains. These chains can form heterotetramers that bind a junctional complex (JC) composed of F-actin, protein 4.1 and the actin-binding proteins dematin, adducin, trompomyosin and tropomodulin. Spectrin and actin are two main structural proteins and, together, form a submembranous cytoskeletal meshwork. It is responsible for the viscoelastic properties of the erythrocyte membrane. Band 3, or the anion channel, other compound of the erythrocyte membrane, is a major transmembranous protein involved in the transport of water and

anions. It is a carrier of the blood-group-I antigen. Glycophorin A, a sialic acid-rich glycoprotein, is the major contact or receptor membrane polypeptide that also spans the lipid bilayer. This network is tethered to the cell membrane at two sites: one mediated by ankyrin, that couples spectrin to band 3, and the other mediated by protein 4.1, that couples the junctional complex to glycophorin C/D (Kim *et al.*, 2015).

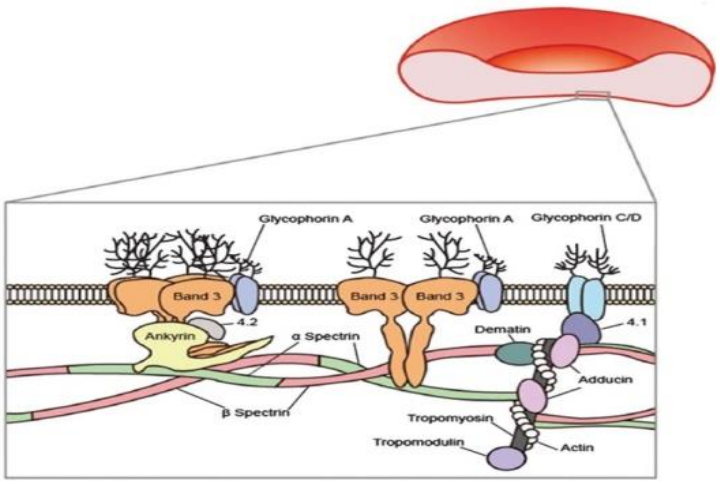

Figure I.4 - The erythrocyte membrane is composed by a lipid bilayer, transmembrane proteins and a filamentous meshwork of proteins that forms a membrane skeleton along the entire cytoplasmic surface of the membrane. Membrane proteins are also asymmetrically oriented within the lipid bilayer and can be divided into three functional sets: structural, catalytic and receptor proteins. Figure from (Kim *et al.*, 2015).

3) Fibrinogen

3.1) Total Plasma Fibrinogen

Fibrinogen is a natural occurring protein in human blood. It is a large, complex and multifunctional plasma glycoprotein synthesised by hepatocytes (Mannila *et al.*, 2007) in the liver that is essential for haemostasis (stopping blood loss from damaged tissues), wound healing, fibrinolysis, inflammation, angiogenesis, cellular and matrix interactions, and neoplasia (Averett & Schoenfisch, 2010; De Oliveira *et al.*, 2012). Normally, fibrinogen in circulation has concentrations ranging from 2 to 4 mg/mL (6-12 µM) (De Oliveira *et al.*, 2012; Ariëns, 2013; Aleman *et al.*, 2014), but people usually carry about 2.5 mg/mL of blood (Xu & Siedlecki, 2009). Sometimes, fibrinogen can circulate in excess, up to 7 mg/mL during acute inflammation (Wolberg, 2016). Fibrinogen is the third most abundant plasma protein and plays a prominent role on the development of surface-induced thrombosis due to its multi-functional role in serving as a ligand for platelet adhesion, linking platelets together into aggregates and stabilizing thrombi by forming a fibrin polymer (Xu & Siedlecki, 2009; Ariëns, 2013). Elevated fibrinogen levels are associated with increased risk of cardiovascular disease, primarily linked to myocardial infarction and stroke (Lovely *et al.*, 2010; Kotzé *et al.*, 2014; Domingues *et al.*, 2016; Wolberg, 2016).

Fibrinogen is a dimeric 340 kDa plasma protein, composed by three pairs of polypeptides chains with bilateral symmetry ($A\alpha_2$, $B\beta_2$ and γ_2) and 29 disulphide bonds (Mannila *et al.*, 2007; Ariëns, 2013). Fibrinogen has an isoelectric point of about 5.5 at physiological conditions (*vd.* Figure I.5).

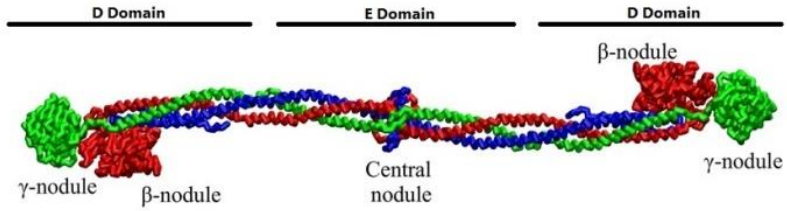

Figure I.5 - Fibrinogen molecule. The polypeptides chain pairs are formed by Aα (blue), Bβ (red) and γ (green). They are oriented so that all six N-terminal ends meet to form the central E domain. Two regions of coiled-coil α helices stretch out on either side of the E domain. Each coiled-coil region ends in a globular D domain, containing the C-terminal ends of Bβ and γ chains, as well as part of Aα chain. The C-terminal end of the Aα chains protrudes from each D domain as a long strand (Mannila *et al.*, 2007; Averett & Schoenfisch, 2010). The β- and γ-nodules are homologous and each of them contains three distinct globular domains. Adapted from (Zhmurov *et al.*, 2011).

Fibrinogen is involved in the coagulation cascade that leads to blood clotting, and it has a rapid response to tissue damage. Blood coagulation is a complex process that involves many collective players and factors. The physiological process of blood clotting and the subsequent dissolution of the clot, after repair of the injured tissue, are essential components of blood haemostasis (Wagner *et al.*, 2013). The coagulation cascade has been divided in two pathways: the intrinsic and the extrinsic pathways, this last one also named tissue factor pathway (Kilinç *et al.*, 2011). After the damage of a vessel wall, there is the exposure of tissue factor (TF) to the bloodstream, initiating a fast cascade system (*vd.* Figure I.6).

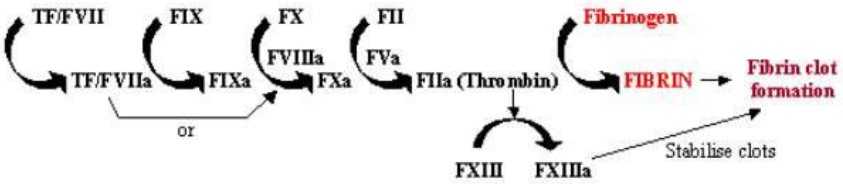

Figure I.6 - Blood coagulation cascade.
(Adapted from http://www.ebi.ac.uk/interpro/potm/2006_11/Page1.htm).

The coagulation cascade begins with a tissue factor, known by thromboplastin, which is a 47 kDa protein expressed in both vascular and nonvascular cells. The tissue factor in circulation activates many other factors initiating the cascade. When the complex is in the presence of factor Va and calcium, factor Xa catalyses the conversion of prothrombin (FII) to thrombin (FIIa). Thrombin converts fibrinogen to fibrin, thereby leading to fibrin deposition, platelet activation and formation of a thrombus (Zhmurov *et al.*, 2011). The activation of factor XIII to factor XIIIa can stabilise blood clots by cross-linking them (Steffel *et al.*, 2006; Kilinç *et al.*, 2011).

Fibrin clots are proteinaceous gels that polymerize in the blood, as a consequence of the biochemical cascade presented above, at sites of vascular injury. Together with platelets, this meshwork stops the bleeding and supports active contraction during wound healing (Brown *et al.*, 2009).

Fibrin is the main contributor for cardiovascular disorders. The plaque rupture can provide a scaffold for thrombi. Clots block blood vessels and cause tissue damage, leading to myocardial infarction, ischaemic stroke, or other cardiovascular diseases (Brown *et al.*, 2009; Stefanelli & Barker, 2015).

The process of conversion of fibrinogen to fibrin, namely the molecular mechanism that occurs when a blood clot is formed, is presented in Figures I.7 and I.8. Fibrinogen contains the central E region or domain, which includes the cleavage sites for thrombin. The E region is connected with two D domains that contain binding pockets important for polymerization. The elasticity of fibrinogen result by the connection of D and E regions through two coiled coil chains (Ariëns, 2013). Both these domains contain important binding sites for the conversion of fibrinogen to fibrin, fibrin assembly and crosslinking, and platelet aggregation. The calcium ions are important to help maintaining the structure of fibrinogen. The N-terminus of Aα and Bβ polypeptides are cleaved by thrombin in order to turn soluble fibrinogen into gel-forming fibrin. Once cleaved from fibrinogen, the N-terminal ends are known as fibrinopeptide A (from Aα polypeptide) and fibrinopeptide B (from Bβ polypeptide). It is known that fibrinogen is a component of the coagulation cascade as well as a determinant in plasma viscosity and erythrocyte aggregation (De Oliveira *et al.*, 2012).

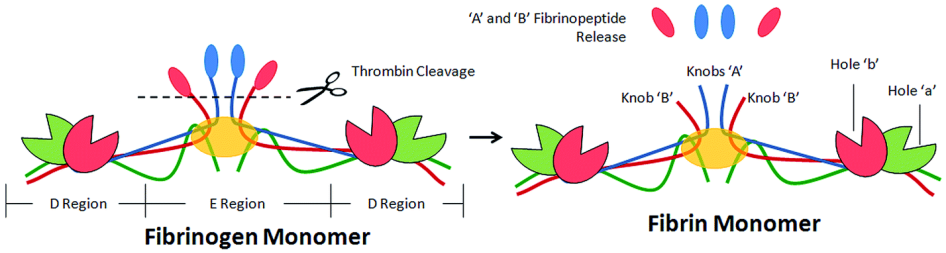

Figure I.7 - Conversion of fibrinogen to fibrin. First, fibrinogen can be cleaved by serine protease thrombin to remove the fibrinopeptides A (blue chain) and B (pink chain), from the central N-terminal disulphide knot ends of Aα and Bβ. This can expose the terminal ends on the E domain, enabling the interaction with the holes ("a" and "b") present on the D domains. Thereby, the fibrinogen monomers are transformed in fibrin. Adapted from (Stefanelli & Barker, 2015).

The Aα protuberances can interact with each other and with the E domain of the fibrinogen molecule during fibrin clot crosslinking (Mannila *et al.*, 2007; Averett & Schoenfisch, 2010). Fibrinopeptide A is cleaved at a faster rate than fibrinopeptide B. Fibrinopeptide A exposes a binding site (GPR) on the fibrin E region for a specific binding of one fibrin molecule with two other fibrin molecules (Ariëns, 2013).

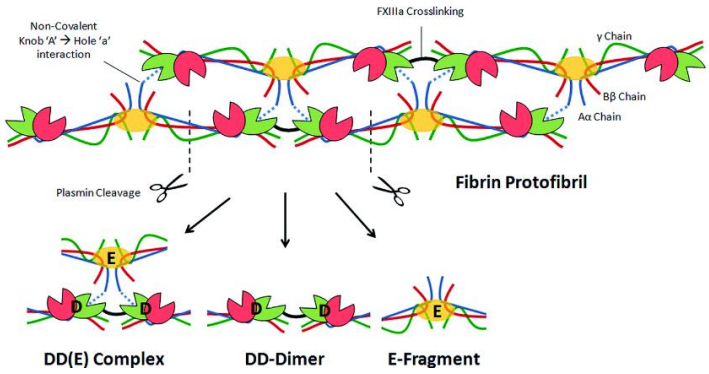

Figure I.8 - Fibrin protofibril formation process. Fibrin molecules can link together through the interaction of the E domain on one fibrin molecule to the D domains on other fibrin molecules, thereby polymerising to form staggered oligomers that build up into protofibrils. The knobs "A" (blue colour) are as prominent as knobs "B"(pink colour) for protofibril formation. The non-covalent knobs "A" are exposed more rapidly, but the knobs "B" are more important for the lateral aggregation of protofibrils. As the fibrin oligomers aggregate, these protofibrils continue to lengthen to make long fibres that can wind around one another to make multi-stranded, thick bundles, and which can branch into a 3-dimentional network of entangled fibres, the fibrin clot. When the transglutaminase factor XIII (FXIIIa) is activated and stabilised subsequently by crosslinking with adjacent D regions within a protofibril form DD-Dimers. This occurs between the C-terminal ends (Aα protuberances) of the Aα polypeptides, as well as (more slowly) at other sites, such as between the C-terminal ends of γ chains (green colour). Only Aα and γ chains become crosslinked by FXIIIa. When fibrin is cleaved by plasmin, the resulting products are DD(E) complex, DD-dimer and E-fragment. Adapted from (Stefanelli & Barker, 2015).

When fibrinopeptide B is cleaved by thrombin, it exposes a second binding site (GHR) in the E region. Other specific binding pocket in the fibrin D region results from the release of the αC region, causing a tether along the fibrinogen E region, which becomes available for intermolecular interactions between fibrin molecules. These interactions contribute to lateral aggregation between protofibrils and fibrin fibres (Stefanelli & Barker, 2015).

When a blood vessel is damaged, platelets prevent the occurrence of extensive bleeding, with the formation of a blood clot, kept together by a dense fibrin network (Carvalho *et al.*, 2015).

The fibrin network structure depends of fibrinogen and thrombin concentration. In the presence of high fibrinogen levels, the density of the fibrin network increases, as well as the clot stiffness, and the resistance of the clots to fibrinolysis (Aleman *et al.*, 2014). Fibrinogen can also mediate platelet aggregation and adhesion. It has two recognition binding sites sequences for platelet receptor: RGD, on the Aα subunits, and a carboxyl-terminal peptide on the γ subunits. The fibrinogen-platelet binding, essential for coagulation, depends on the platelet membrane receptor glycoprotein $\alpha_{IIb}\beta_3$ (Carvalho *et al.*, 2011). This is the major integrin on platelets. It is essential for platelets aggregation and is centrally involved in haemostasis and thrombosis (Ma *et al.*, 2007).

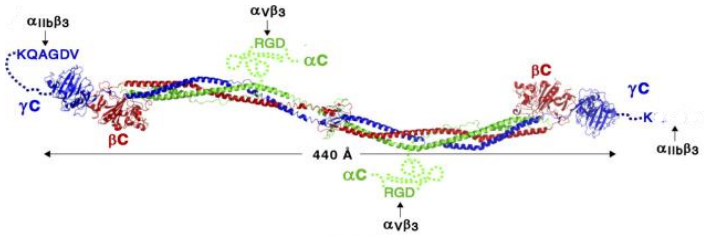

Figure I.9 - Fibrinogen molecule with different recognition binding sites for distinct integrin receptors ($\alpha_{IIb}\beta_3$ and $\alpha_V\beta_3$). Adapted from (Springer *et al.*, 2008).

Increased fibrinogen concentration and erythrocyte aggregation are factors that significantly increase the risk of cardiovascular and cerebrovascular diseases. Fibrinogen binding to the $\alpha_{IIb}\beta_3$ receptor requires calcium to activate the integrin complex. The effect of the absence of calcium is more pronounced for the fibrinogen-platelet system than for erythrocytes. Thus, the erythrocyte receptor for fibrinogen, is not as calcium dependent and as influenced by the presence of the eptifibatide as the platelet receptor. Its inhibition by eptifibatide indicates that the receptor for fibrinogen on erythrocytes is not the glycoprotein $\alpha_{IIb}\beta_{3,}$ but a related integrin (Carvalho *et al.*, 2010).

It is known that the arterial thrombi have high levels of platelets and venous thrombi are mostly constituted by erythrocytes and fibrin (Aleman *et al.*, 2014). In blood clot formation, erythrocytes are the major component of the thrombus. Venous thromboembolism is the third most common cardiovascular illness, after acute coronary syndrome and stroke (Wagner *et al.*, 2013).

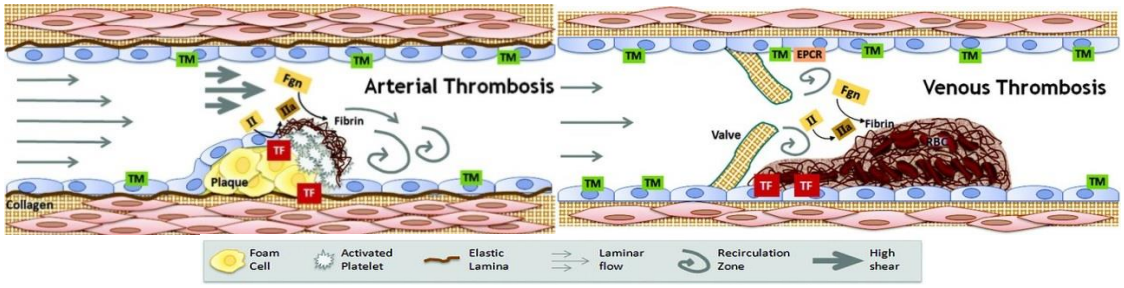

Figure I.10 - Clots on arterial thrombosis can be called white clots, because they are mainly constituted by platelets. Accordingly, clots on venous thrombosis can be called red clots, due to their content in erythrocytes and fibrin (Aleman *et al.*, 2014). TM – thrombomodulin; EPCR – endothelial protein C receptor; II – prothrombin; IIa – thrombin; TF – tissue factor; Fgn – fibrinogen; RBC – red blood cells.
(Figures from https://www.med.unc.edu/wolberglab/images/arterial%20thrombosis.jpg/@@images/83373353-123c-476d-af5c-97773048fac3.jpeg and https://www.med.unc.edu/wolberglab/images/venous%20thrombosis.jpg/image_preview).

3.2) γ' Fibrinogen

Fibrinogen in plasma is a heterogeneous mixture of isoforms with different relative proportions. Fibrinogen variants are the result of alternative splicing of the γ-chain. mRNA processing and post-translational modifications give rise to several different fibrinogen isoforms with widely varying characteristics. The γ' isoform arises from alternative mRNA processing, leading to the substitution of the last 4 amino acid residues of the carboxyl terminal, by another 20-amino acid residues sequence. This is originated by the introducing of 20 new residues at the γ-chain C terminus by the open reading frame from intron 9, replacing 4 residues encoded by exon 10 followed by a stop codon. Thus, the fibrinogen γ chain has 2 isoforms: the gamma A (γA or simply γ) isoform and the gamma-prime (γ' or γB) isoform. Therefore, at the level of the γ-chain the fibrinogen molecule can be a homodimer (γA/γA) that constitutes approximately 84% of the total plasma fibrinogen concentration, an heterodimer (γA/γ') that are present in approximately 15% or an homodimer (γ'/γ') that constitutes the remaining 1% of fibrinogen concentration (Lovely *et al.*, 2010; Ariëns, 2013; Domingues *et al.*, 2016; Macrae *et al.*, 2016).

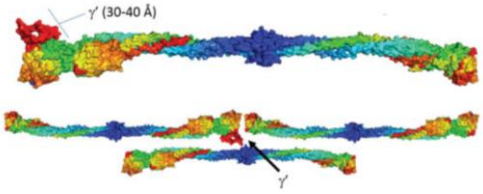

Figure I.11 - Proposed model of the γ'-chain of the fibrinogen molecule. The 20 amino acid extension of the γ′-chain is located at the C-terminus, on the D region of the fibrinogen molecule (red region). The 20 amino acid may extend the fibrinogen molecule 30 to 40 Å. Figure from (Macrae *et al.*, 2016).

The γ' fibrinogen has several biochemical and biophysical properties that distinguish it from the more common γA isoform. This fibrinogen variant, has been reported to have more affinity on the binding to thrombin (Ariëns, 2013). It has been associated with a non-uniform clot structure with prolonged clot lysis time (Kotzé *et al.*, 2014) and with various biological functions which are disclosed upon fibrin clot formation. When the fibrin clots are formed in the presence of γ'-chain fibrinogen variant, they are most resistant to fibrinolysis (Mannila *et al.*, 2007; Domingues *et al.*, 2016). Furthermore, the γ' chain contains a binding site for thrombin, and clots made from γ' fibrinogen have been reported to have altered clot architecture. γ' fibrinogen forms thinner but denser fibrin fibres. Possibly as a result of these properties, recent studies suggest that γ' fibrinogen is a risk factor for cardiovascular disease. This fibrinogen variant has been associated with the extent and severity of coronary artery disease and an increase risk of arterial thrombosis, myocardial infarction and stroke (Mannila *et al.*, 2007; Domingues *et al.*, 2016; Macrae *et al.*, 2016).

4) *Amyotrophic Lateral Sclerosis*

Amyotrophic lateral sclerosis (ALS) is a devastating and fatal neurodegenerative disorder, characterized by rapid and progressive degeneration of motor neurons in the spinal cord, brainstem and motor cortex (Pronto-Laborinho *et al.*, 2014), which results in muscle atrophy, paralysis and death (D'Angelo *et al.*, 2013). ALS patients die mainly from respiratory failure, related to weakness of diaphragm and other respiratory muscles (Pronto-Laborinho *et al.*, 2014).

The worldwide incidence of ALS is between 1.5 and 2.5 per 100,000 persons per year, with a male/female ratio of 3:2. Most patients have first symptoms between 55-65 years and the median survival expectancy of ALS patients is 3-5 years after symptom onset (Pronto-Laborinho *et al.*, 2014; Kioumourtzoglou *et al.*, 2015).

Most ALS cases are sporadic (SALS) (90-95%); the remaining 5-10% of patients have a positive family history for ALS or frontotemporal dementia (FALS) (Pronto-Laborinho *et al.*, 2014; Kioumourtzoglou *et al.*, 2016). More than 16 dysfunctional genes have been described in FALS, and approximately 20% of FALS patients have a missense mutation in the gene encoding the enzyme Cu/Zn super oxide dismutase (SOD1) (Pronto-Laborinho *et al.*, 2014).

ALS can have spinal, bulbar, respiratory, axial or diffuse form. ALS cases increase with increasing age (Kioumourtzoglou *et al.*, 2015).

Riluzole is the only drug currently approved in ALS, acting by decreasing glutamate activity in the central nervous system, which increases life expectancy on about 3-6 months. The etiology of ALS pathogenesis is complex and not completely understood. The mechanisms of the disease comprises oxidative stress, excitotoxicity, protein aggregates, mitochondrial dysfunction, neuroinflammation, cytoskeletal derangements, deregulated growth factors, impaired axonal transport and apoptosis, abnormal calcium metabolism and activation of proteases and nucleases (Pronto-Laborinho *et al.*, 2014).

Several clinical prognostic factors have been identified in ALS, such as age, site of onset, functional and respiratory status, cognitive function, non-invasive ventilation, some genetic mutations, and clinical phenotypes (Chiò *et al.*, 2014; Kioumourtzoglou *et al.*, 2015).

Previously, the main causes of death in ALS patients were respiratory problems, including respiratory muscle paralysis and bronchopneumonia (Tanaka *et al.*, 2013). Some patients with respiratory-dependent ALS die of sudden cardiac arrest or anoxic encephalopathy following circulatory collapse, which may be associated with sympathetic hyperactivity (Tanaka *et al.*, 2013). However, recent studies, related that exist an inverse association between cardiometabolic health and ALS disease (Kioumourtzoglou *et al.*, 2015).

Other studies have demonstrated a protective association between ALS incidence and cardiovascular risk factors such as obesity, higher cholesterol levels and hyperlipidaemia. Diabetes has been associated with high levels of uric acid that prolonged survival in ALS (Kioumourtzoglou *et al.*, 2015,

2016). Various biomarkers have been proposed as potentially related to a better ALS outcome, including dyslipidaemia, elevated levels of uric acid and creatinine, and reduced granulocyte count (Chiò *et al.*, 2014).

Venous Thromboembolism (VTE), a cardiovascular risk, is also associated with ALS disease. Neurologic diseases that affect lower limb function are described as risk factors for venous thromboembolism. ALS has several risk factors for VTE, such as reduced mobility, increased age and progressive respiratory failure. Thus, VTE is common in ALS patients (Gladman *et al.*, 2014). Therefore, VTE is considered as a complication of ALS, and it is highly correlated with leg functions (Berry & Korngut, 2014).

On another study, performed by Namazi *et al.* (2014), one ALS patient was diagnosed with heart failure at the final stage of the disease. However, the association between ALS and cardiovascular disease is rare and underdiagnosed, because symptoms are masqueraded as a result of the patients' disability. Cardiac denervation related to involvement of the sympathetic nervous system has been depicted in patients in the early stages of ALS. Other studies indicated some metabolic abnormalities in central nervous system and systemic circulation. The sympathetic hyperfunction and vagal hypofunction of the cardiovascular system have a subclinical role in ALS patients (Chida *et al.*, 1989).

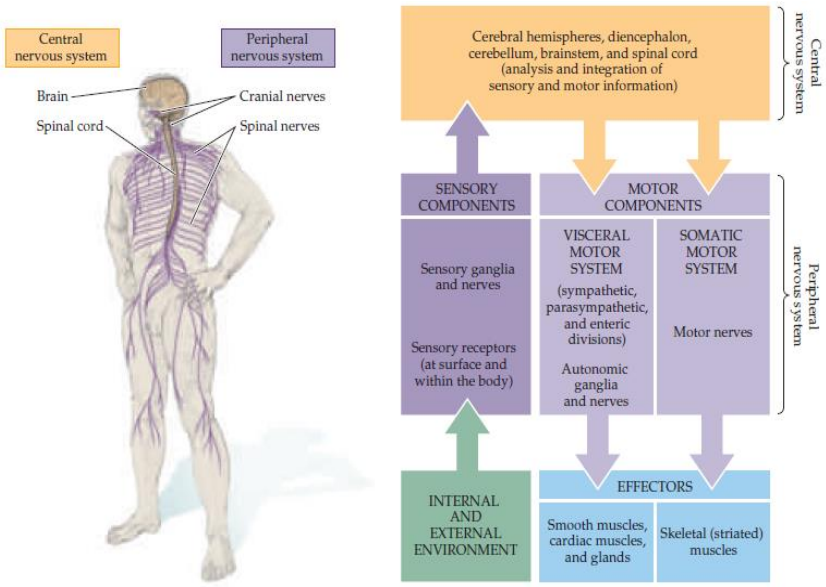

Figure I.12 - Regions of the nervous system that can be affected in ALS disease. All the nervous system has interrelation and when the upper and lower motor neurons undergo degeneration, other components can also be affected (Purves *et al.*, 2004).

The motor neuron disease (MND) phenotype, that has been described to involve the sympathetic nervous system, can also be attributable to cardiac denervation in patients in the early stages of ALS. This result is related with the fact that the levels of norepinephrine and epinephrine are increased in ALS patients (Gdynia *et al.*, 2006). Symptoms of an autonomic dysfunction are not a characteristic of ALS, although there are reports of cardiac arrhythmia (Sachs *et al.*, 1985).

ALS can also lead to total paralysis and respiratory failure. Knowing that ALS patients frequently have respiratory failure, the diagnosis and treatment of cardiac arrhythmias revealed to be difficult. ALS affects the autonomic nervous system, which contributes for regulation of heart rate, blood pressure and others homeostatic functions. Thus, the cardiovascular autonomic dysfunction contributes to the morbidity of the disease. As previously described, sympathetic predominance with vagal withdrawal tends to occur in early stages of ALS disease. At these stages of the disease, the most common symptom is sinus tachycardia. Bradycardia results from sympathetic denervation. However, in advanced ALS, the spinal cord sympathetic ganglia (known as the intermediolateral nucleus) also undergo degeneration. In addition to late central sympathetic failure, there is also degeneration of peripherally mediated sympathetic nerves (Shemisa *et al.*, 2014).

5) *Atomic Force Microscopy*

Atomic Force Microscopy (AFM) is a technique that can be used for high-resolution real-time studies. It can both measures properties of molecules at the nanoscale and of dynamic changes in biological systems, such as cells, viruses and bacteria (Kim *et al.*, 2003; Karagkiozaki *et al.*, 2008; Variola, 2015). AFM has contributed to nanomedicine with developments in nanodiagnostics and nanotherapeutics, contributing to the improvement of relevant healthcare processes (Carvalho *et al.*, 2015).

Atomic force microscopy is a surface probe technique that uses a soft cantilever to image surfaces or to measure or apply forces while interacting with them (Cazaux *et al.*, 2016). AFM key element is a small and flexible cantilever controlled in the z-direction by a piezoelectric crystal. The cantilever acts like a spring to measure the force between the tip and the sample's surface (Averett & Schoenfisch, 2010). The sharpened tip is brought into contact with the sample and moved across the surface. The instrument measures the deflection of the cantilever as it scans, and from this information about the tip movement a pseudo-three-dimensional image of the sample is built up (JPK Instruments AG, 2012; Variola, 2015) (*vd.* Figure I.13a).

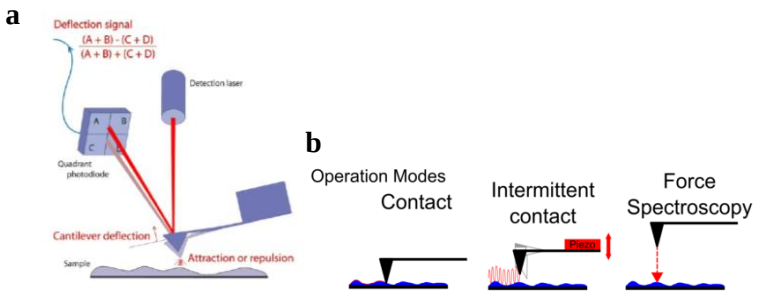

Figure I.13 - AFM principles. **(a)** The deflection of the cantilever is detected and processed as a function of the position on the (x, y) plane, in order to obtain topographical images (JPK Instruments AG, 2012). **(b)** AFM operation modes. The AFM can operate in a variety of modes, including contact, intermittent contact and force spectroscopy (Variola, 2015). (Adapted from http://static1.squarespace.com/static/51acda21e4b0be9ceadc57b3/t/538c8e2be4b01a84edc5f741/1401720367289/).

The AFM can operate in different modes. The tip can be continuously contacting with the sample's surface (contact mode), or the cantilever could be oscillating and the variations on its resonance frequency are used to generate images (intermittent contact or tapping mode). On this mode, the cantilever moves rapidly with a large oscillation between the repulsive and attractive forces (*vd.* Figure I.13b). An optical lever is created by a beam of light from a light-emitting diode reflected off of the cantilever onto a position-sensitive photodiode (Averett & Schoenfisch, 2010). Deflections of the cantilever cause changes in the position of the light spot, and may be translated into applied force using Hooke's Law:

$$F = -K\Delta x \qquad (1)$$

Thus, a cantilever deflection *vs.* scanner displacement curve can be converted into a force-distance curve (Carvalho & Santos, 2012). This means that the force (F) needed to extend the cantilever spring

constant (K) depends in a linear way of the cantilever deflection (Δx) that may extend it (JPK Instruments AG, 2012) (*vd*. Figure I.14). When the tip contacts the sample at a given point, the cantilever can move vertically and the deflection of the cantilever provided information on the mechanical properties of the sample's surface or on the tip-sample interactions (force spectroscopy mode).

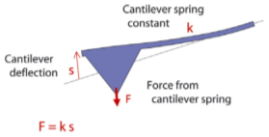

Figure I.14 - Scheme of the AFM process and how to apply the Hooke's Law to calibrate the cantilever (JPK Instruments AG, 2012).

5.1) Atomic Force Microscopy Applications

5.1.1) Cell Imaging

Atomic force microscopy has been usually applied to characterize the nanometric features of the surfaces of samples and also to map the spatial distribution of their physicochemical properties. AFM has the capacity to visualize nanotopographical features and correlate them to surface charge density and electrical characteristics of the biomaterials. The contact and oscillation modes are most commonly used to image reconstituted membrane proteins and native membranes (Fotiadis, 2012). The AFM technique involves a small sensor scanning over the surface of the cell. AFM is typically an imaging technique in which the surface of a sample is scanned, line by line, by the movement of a thin tip mounted on a flexible cantilever. The tip-sample repulsion at the atomic level, transduced by the cantilever deflection and by an optical lever mechanism allows the association of a height value to each position on the x,y plane, enabling the reconstitution of a high-resolution pseudo-three-dimensional image of the sample surface (Carvalho *et al.*, 2015). AFM has the capacity of imaging, in air or in liquid, nonconductive and conductive surfaces beyond the light diffraction limit, reaching molecular and atomic resolution for some samples (Averett & Schoenfisch, 2010). Operating in contact mode, the force applied by the tip is constantly adjusted manually to image the sample in a non-perturbed state. In oscillation mode (intermittent contact), the cantilever is rapidly oscillated in the vertical direction while raster scanning the sample. Ideally, the AFM tip then only touches the sample on its downward movement and is not in constant contact with the sample as in contact mode. The 'tapping' mode has the advantage that lateral forces and friction are virtually eliminated. Hence, the oscillation mode is particularly convenient for AFM imaging of soft and weakly adsorbed biomolecules. However, in spite of this considerable advantage, contact mode-AFM imaging still remains the operating mode of choice to achieve high resolution on native and reconstituted membrane protein surfaces (Fotiadis, 2012). AFM imaging of cells generates relevant structural information, allowing the identification of functional components on cells, and giving information about the

heterogeneity of the cell surface in terms of protein composition and distribution (Fotiadis, 2012; JPK Instruments AG, 2012; Variola, 2015).

5.1.2) Atomic Force Microscopy-based Force Spectroscopy

AFM-based Force Spectroscopy allows the measurement of inter and intramolecular interaction forces required to separate the tip from the sample, with piconewton (pN) resolution. Thus, the AFM can be used to quantify the interaction between the tip and a specific spot of the sample, taking advantage of the piconewton sensitivity of the method (Averett & Schoenfisch, 2010; Carvalho & Santos, 2012; Carvalho *et al.*, 2015).

The interaction force depends on the nature of the samples, the probe tips and the distance between them. It measures the interaction force between a sharp tip and a surface, or may vibrate as it moves along it. The design of a force-distance curve depends on these characteristics and of the composition of the medium. There are differences in curves obtained for measurements in air and in liquid medium. In force spectroscopy measurements, the cantilever moves in the vertical direction (z axis) toward the surface and then in the opposite direction. During this procedure, the cantilever deflection as a function of the vertical displacement of the piezoscanner can be recorded. The result is a cantilever deflection *versus* scanner displacement curve, which can be converted into a force-distance curve after applying the Hookes's law of elasticity (Carvalho & Santos, 2012) (*vd.* Figure I.15). To obtain the quantitative parameters, the accurate calibration of the spring constant of the cantilevers is necessary (Averett & Schoenfisch, 2010). This technique can be used a highly sensitive nanotool for the diagnostic and unbiased functional evaluation of the severity of haematological diseases arising from genetic mutations. AFM-based force spectroscopy can be used to measure the binding force between fibrinogen and cell receptors and for the identification of the fibrinogen receptor on erythrocytes (Carvalho *et al.*, 2010). Different types of forces can be studied using AFM-based force spectroscopy, both attractive and repulsive (Carvalho *et al.*, 2013).

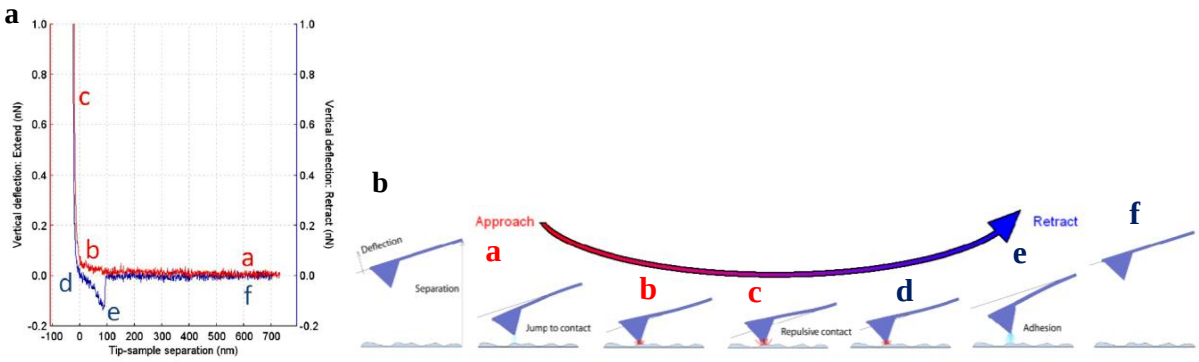

Figure I.15 - AFM-based force spectroscopy. **(a)** Schematic representation of the force-distance curve obtained by AFM-based force spectroscopy, showing a single adhesion event. The red line is the approach curve and the blue line is the retraction curve. **(b)** Diagram of the vertical tip movement during the approach and retraction curves of force spectroscopy measurements. The letters represent different moments during the approach and retraction curves. Adapted from (JPK Instruments AG, 2012; Carvalho *et al.*, 2013).

In Figure I.15, the cycle begins with the tip away from the cell surface (a) and the forces measured by the cantilever deflection can change as it is moved toward or away from the sample on its neutral position (0 pN). From this position, the tip starts moving down towards the surface, reaching the contact point (b). On the approach curve, the van der Waals interactions are the main type of force present on the approaching of two hard surfaces in the absence of long-range interactions. This force is characterized by a small deflection of the cantilever, at the approach curve, before the contact point. The jump to contact causes instability in the position of the cantilever because it occurs when the gradient of force between the tip and the sample exceeds the stiffness of the cantilever. If the approach curve has a smooth and exponentially increasing repulsive force, it is expectable that electrostatic or polymer-brush forces are present. Viscoelastic properties of some biological systems have been determined using AFM force curves. There is a waiting time before starting the retraction curve and another after reaching the defined applied force (c). Afterwards, tip and cantilever begin the upward movements away from the sample, in the opposite direction, reaching the contact/adhesion point (d). In the retraction curve, an adhesion force profile, the force depends on the type of the sample and appears as a deflection of the cantilever below the zero-deflection line (e). The central basis of adhesion forces is the development of a capillary bridge between the tip and the sample. This capillary force depends if the measurements are made in air or in liquid. In air, samples usually have several nanometers of water molecules adsorbed to their surface. In liquid conditions, the adhesion force not only depends of the interaction energies between tip and sample but also on the type of solution used. If no adhesion occurs between the molecules attached to the tip and the cell surface, the tip continues its upward movements, at 0 pN of force, and reaches back the neutral position at a defined z distance point (f). If a bond is formed between the tip and the sample, as the cantilever moves upward, it bends down to negative values in force. To quantitatively analyse force-distance curves, it is necessary to accurately calibrate the spring constant of the cantilevers. Cantilever stiffness depends on the shape and on the material properties of the cantilevers (JPK Instruments AG, 2012; Carvalho *et al.*, 2013).

5.1.2.1) Force Spectroscopy modes

The AFM-based force spectroscopy can be used at diverse applications. The main application modes that were applied on this study were molecular interaction, adhesion and indentation.

Molecular interactions studies

Single-molecule force spectroscopy (SMFS) is an extremely powerful tool for detecting and localizing single molecular recognition events, and for exploring the energy landscape of molecular interactions. Different molecules, or their domains, can be attached to the tip, and each part of the molecule can break contact separately or altogether (Carvalho *et al.*, 2013). After attaching a molecule to the tip and/or to the sample surface, the unfolding, stretching, or adhesion of single molecules can be studied.

The tips are commonly functionalized with one or a small amount of molecules. These molecules can recognize a specific target molecule on the sample surface. When analysing the stretching of biomolecules, and in order to measure specific and strong interactions between tip and sample, it is necessary to specifically attach to the tip the biomolecule under study. The attachment should be firm enough to avoid reallocations, but it should maintain some autonomy of the molecule to change its conformation during or before the interaction (Carvalho *et al.*, 2013). The simplest method to attach molecules to the tip is via their non-specific adsorption. However, the covalent attachment methods usually yield better performances. With this process, parameters like stiffness, persistence length, and inter- or intramolecular transitions can be studied. Proteins can be unfolded in a controlled way, to explore the structure of the molecule (Carvalho *et al.*, 2013).

Indentation studies

AFM-based detection of stiffness is highly dependent on the appropriate use of theoretical models. Cells elasticity can be measured by nanoindentation with the most common AFM cantilevers, via the Hertzian theory (Carvalho & Santos, 2012). This theory of elastic contact is the most widely used approach to estimate the elastic properties of cells from force indentation curves, using the depth of indentation to assess elasticity in terms of the Young's elastic modulus. Specifically, this method allows characterizing the elasticity of biological structures, comparing different types of cells or even organelles. Experimental conditions concerns the indenters' shape or the thickness of the sample (Carvalho & Santos, 2012).

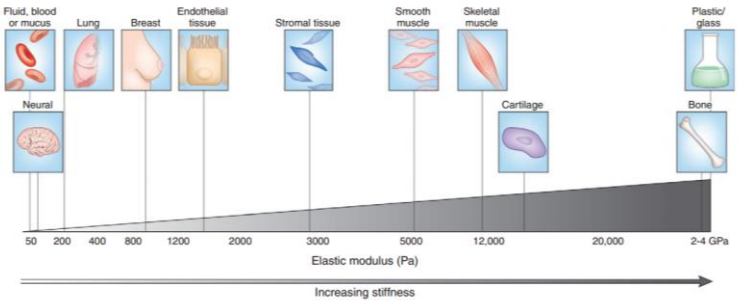

Figure I.16 - Variations in tissue stiffness. The biomechanical properties of a tissue in terms of stiffness (elastic modulus), measured in Pascal (Pa), vary markedly between organs and tissues, and are inherently related to tissue function (Cox & Erler, 2011).

Single-cell adhesion studies

Atomic force microscopy-based single-cell force spectroscopy (SCFS) is used to quantify the contribution of cell adhesion molecules to the adhesion of cells to specific substrates both at the cell and at a single molecule level. In AFM-based SCFS, a single cell is attached to a cantilever, commonly facilitated by an adhesive coating (*e.g.*, concanavalin A, poly-L-lysine or CellTak). The attached cell is brought into contact with a substrate, which can be a protein-coated surface, another

cell or a biomaterial, until a set force is reached. The cell is kept stationary in contact with the surface for a set of time to allow the formation of adhesive interactions. During the subsequent retraction of the cantilever, the force acting on the cell and the distance between cell and substrate are recorded in a force-distance curve. The force values that can be detected with AFM-based SCFS are from ~10 pN up to ~100 nN. Thereby, SCFS allows both the overall cell adhesion and the contribution of single adhesion receptors to be quantified. During cantilever retraction, the upward acting force on the cell increases until the force needed to initiate cell de-adhesion is reached, leading to unbinding events (*vd.* Figure I.17). At the cellular level, single cells can be ingeniously fixed onto the cantilever, becoming the probe for the dynamic quantification of cell–substrate interactions (SCFS). Parameters such as maximum detachment force and work for the entire cells as well as a number of detachment events of single cellular tethers have already been successfully quantified. The maximum force is called the adhesion force and it is a measure of how strong cell adhered to the substrate. Unbinding events can be characterized either as rupture (jumps) or membrane tether events. The analysis of these unbinding events may be used to characterize the strength of single bonds and cell membrane properties (Bowman *et al.*, 2012; Yu *et al.*, 2015).

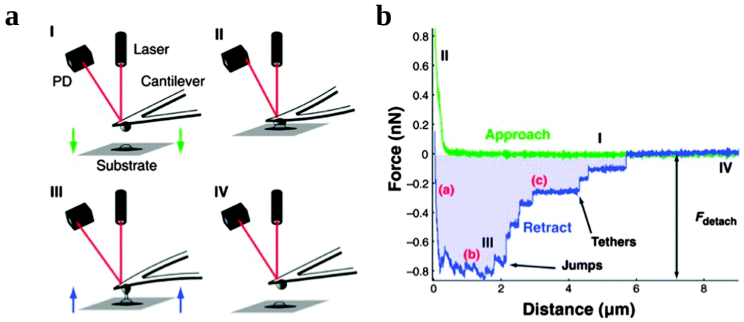

Figure I.17 - Schematic overview of AFM-based cell-cell adhesion experiments **(a)**. Force-distance curve showing maximum detachment force (F_{detach}), work necessary for the cell detachment from the substrate (shaded area) and two types of molecular unbinding events: (I) the receptor remains anchored in the cell cortex and unbinds as the force increases (designed as jumps) and (II) receptor anchoring is lost and membrane tethers are pulled out of the cell **(b)**. Image from (Variola, 2015).

Adhesion is a fundamental aspect of cells, both in health and disease. In the last decade, single cell adhesion studies have contributed to the understanding of adhesion proteins and their regulation. AFM-based SCFS has been used to quantify adhesion of numerous cell types to a diverse set of substrates, include extracellular matrix (ECM) proteins, biomaterials and cell–cell adhesion proteins (Yu *et al.*, 2015).

II) Objectives

The two main goals of this thesis were:

i. To study the influence of fibrinogen molecules on erythrocyte-erythrocyte adhesion of stroke patients.
ii. To evaluate morphological and elasticity changes on erythrocytes from patients with Amyotrophic Lateral Sclerosis.

III) Material and Methods

1) Blood collection

Human blood cells were obtained by vein puncture from healthy adult volunteer donors (n=57), used as control. The blood collection was performed at Instituto Português do Sangue e da Transplantação de Lisboa, Portugal, under an institutional agreement with Instituto Português do Sangue (Lisbon). Human blood cells were also obtained by vein puncture from stroke patients and from Amyotrophic Lateral Sclerosis patients in a close collaboration with clinicians from Serviço de Medicina I (Prof. Carlos Moreira) and Serviço de Neurologia (Prof. Mamede de Carvalho), respectively, from Santa Maria Hospital (Centro Hospitalar Lisboa Norte). Healthy donors, stroke and ALS patients samples were obtained with their previous written and signed an informed consent, or from their proxy, as approved by the joints Ethical Committee of Santa Maria Hospital and of the Faculty of Medicine of the University of Lisbon.

Blood samples from healthy donors (control) and stroke patients were collected into K_3EDTA, lithium heparin and sodium citrate 3.8% anticoagulant tubes (Vacuette, Greiner Bio-One, Germany) and ALS patients were collected into S-Monovette 4.9 mL, Lithium heparin and K_3EDTA anticoagulant tubes (Sarstedt, Germany).

K_3EDTA, heparin and sodium citrate anticoagulant tubes were used according to the different measurements performed to analyse hematologic and haemorheological parameters. K_3EDTA is a critical factor of coagulation and is particularly useful for haematological examination, being the tri-potassium salt the most stable. This anticoagulant prevents platelet aggregation, conserves blood cells properties and blocks the formation of prothrombin and the beginning of the coagulation process. It is used for haemogram and for erythrocyte isolation.

Heparin is the most widely used anticoagulant for clinical chemistry analysis, because it binds to several enzymes responsible for the coagulation cascade. It is present naturally in blood and prevents blood cells haemolysis. Heparin tubes were used for analysing haemorheological parameters and for fluorescence generalized polarization measurements.

Sodium citrate is widely used for coagulation studies. The effect is easily reversible by the addition of Ca^{2+}. It was used for total fibrinogen and γ' fibrinogen quantification in plasma (Mafuvadze & Erlwanger, 2007; Gonzalez-Covarrubias *et al.*, 2013).

2) *Haemogram*

Haemogram were quantified using whole blood collected into K_3EDTA anticoagulant tubes. Analysis were done on a Haematological Analyser (PocH-100iV - Hematology Analyzer, Sysmex Europe GmbH, Hamburg, Germany). Haemogram allows the counting of each of the human blood cells elements and to compare these results with reference ranges for each parameter. About 40 to 45% of the blood volume is occupied by erythrocytes. This percentage of volume is termed haematocrit (Baskurt & Meiselman, 2003).

3) *Human Blood Cells Isolation*

For human blood cells isolation, the blood was collected into K_3EDTA anticoagulant tubes (3mL) and cells were isolated as previously described elsewhere (Carvalho *et al.*, 2015). In a refrigerated centrifuge (Heraeus Multifuge 1 L-R, Thermo Scientific, UK), blood was centrifuged at 1620 *g* for 10 min, at 10ºC, resulting in a three phase solution: an upper phase of plasma, a middle phase of buffy-coat and a lower phase of erythrocytes.

The supernatant (plasma and buffy coat) was discarded and the erythrocytes were resuspended in 1 mL of buffered saline glucose-citrate (BSGC) buffer (1.6 mM KH_2PO_4, 8.6 mM Na_2HPO_4, 0.12 M NaCl, 13.6 mM sodium citrate, and 11.1 mM glucose) pH 7.3 with $CaCl_2$ (1 mM). On the second centrifugation, the supernatant was disposed, without buffer addition, and the erythrocyte mush was kept at 4ºC, until further use.

4) *Atomic Force Microscopy*

A NanoWizard II atomic force microscope (JPK Instruments, Berlin, Germany) mounted on the top of an Axiovert 200 inverted optical microscope (Carl Zeiss, Jena, Germany) was used for imaging and force spectroscopy experiments during this project.

4.1) AFM Scanning Images of Human Blood Cells

The AFM head is equipped with a 15 μm z-range linearized piezoelectric scanner and an infrared laser. Imaging of the erythrocytes was performed, in air, in tapping mode. Oxidized sharpened silicon tips with a tip radius of ~ 6 nm, resonant frequency of about 60 kHz and spring constant of 3 N/m were used for the imaging. Imaging parameters were adjusted to minimize the force applied on the scanning of the topography of the cells. Scanning speed was optimized to 0.3 Hz and acquisition points were 512×512. Imaging data were analysed with the JPK Image Processing software v.5.1.8

(JPK Instruments, Berlin, Germany). The diameter, area, height and volume of each imaged cell were quantified using the SPIP software v.6.6.0 (Image Metrology, Hørsholm, Denmark). The roughness of the erythrocytes was also analysed by Gwyddion software v.2.45 (Czech Metrology Institute, Czech Republic) (Carvalho *et al.*, 2010; Bernardes *et al.*, 2016).

4.2) AFM – based Force Spectroscopy

For the AFM experiments, the erythrocytes were isolated from the blood plasma. Then the cells were suspended into final 0.1% haematocrit with saline glucose-citrate (BSGC) buffer (1.6 mM KH_2PO_4, 8.6 mM Na_2HPO_4, 0.12 M NaCl, 13.6 mM sodium citrate, and 11.1 mM glucose) pH 7.3 with $CaCl_2$ (1 mM). After this, the solution was placed on a poly-L-lysine-coated glass slide and erythrocytes were allowed to adhere firmly for 30 min (Carvalho *et al.*, 2010, 2011, 2015; Guedes *et al.*, 2016).

AFM indentation for elasticity

For erythrocyte indentation experiments, non-functionalized OMCL TR-400-type silicon nitride tips (Olympus, Japan) were used. The softest triangular cantilevers, with a tip radius of ~15 nm and a resonant frequency of 11 kHz, were used. The spring constants of the tips were calibrated by thermal fluctuation method having a nominal value of 0.02 N/m. For every contact between the cell and the cantilever, the distance between the cantilever and the cell was adjusted to maintain a maximum applied force of 300 pN for erythrocytes from ALS patients before retraction. Cell elasticity was measured on one point of each erythrocyte (5 force-distance curves per cell). Data collection for each force-distance cycle was performed at 1.5 Hz, with a z-displacement range of 4 μm. Force curves were made at the centre of the cell. Data acquired on the nanoindentation experiments (force curves) were analysed to obtain the cells Young's modulus (E), using JPK Image Processing software v.5.1.8, by the application of the Hertzian model. The probe was modelled as a quadratic pyramid, with a tip angle of 35º (half-angle to face) and a Poisson ration of 0.50. Histograms results of the Young's modulus were constructed for each experimental condition studied. The ideal histogram bin size was chosen in order to achieve the best fitted Gaussian model peak length. The maximum values of the Gaussian peaks represent different statistical measure of the Young's modulus of the cells. AFM tip penetration depth onto erythrocytes was also evaluated. This parameter was analysed by the position of the maximal movement of the piezo sensor in the z-axis, which corresponds to the z-axis coordinate when the sensor reaches an indentation force of 300 pN for erythrocytes from ALS patients, subtracting the z-axis position of the sensor when the tip begins the contact with the surface of the erythrocyte (Guedes *et al.*, 2016).

Protein-cell interactions

Force spectroscopy measurements were performed on the same equipment using fibrinogen functionalized OMCL TR-400-type silicon nitride tips (Olympus). The softest triangular cantilevers,

with a tip radius of ~15 nm and a resonant frequency of 11 kHz, were used. For the functionalization, AFM silicon nitride tips were cleaned with an intense ultraviolet light source and silanized in a vacuum chamber with 3-aminopropyl-triethoxysilane (APTES, 30µl) and N,N-diisopropylethylamine (10 µl) for 1 hour in an argon atmosphere. Amine-terminated AFM probes were then placed in glutaraldehyde solution 2.5% (v/v) for 20 min and washed 3 times with PBS (phosphate buffered saline) pH 7.4. Finally, the tips were placed into fibrinogen solution to attach the fibrinogen molecules. Purified human fibrinogen (Sigma Aldrich, USA) was used at a concentration of 1 mg/mL with an incubation during 30 min. Fibrinogen-functionalized tips were immediately mounted on the atomic force microscope and used for the force spectroscopy measurements (Carvalho *et al.*, 2011, 2015). Cantilevers with a nominal spring constant of approximately 0.02 N/m were used after their calibration using the thermal fluctuation method. The applied force was adjusted to 800 pN, before retraction. Data collection for each force-distance cycle was performed at 3 µm/s, leading to an average loading rate of ~9 nN/s. For each blood sample, approximately 3000 force *vs.* distance curves were collected, analysed and adjusted by polynomial fit by JPK Image Processing software v.5.1.8 (JPK Instruments, Berlin, Germany).

Cell-cell adhesion

In these AFM studies, a 100 µm long range force-spectroscopy was made possible by the development of the CellHesion® module for the BioAFM NanoWizard® (JPK Instruments). They created an integrated system for measuring cell-cell and cell-substrate interactions. The objective was mounted with a PIFOC® focus tracking system that allows the user to keep the plane of interest in focus at all times during the experiments and to enable concurrent movement of the objective with the sample holder during force spectroscopy measurements. Tipless cantilevers (Arrow TL1, NanoSensors) with 1µm of thickness, 0.03 N/m of spring constant and 7 kHz of resonance frequency were used. For this study the cantilevers were functionalized for attached the cell to the cantilever, through the cell capture, a semi-automatic approach system. The process of the cantilever functionalization for use in erythrocytes was based in the work of Wojcikiewicz *et al.* (2004). This method has good acceptance since the streptavidin/biotin system has been well characterized. This complex has high-affinity, and the initial layer of biotin-BSA (biotinylated bovine serum albumin) may help to mask any electrical charges on the cantilever tip that could lead to nonspecific binding.

For the functionalization, AFM cantilevers were cleaned with an intense ultraviolet light source for 15 min. After this, the cantilevers were incubated in a 50 µl drop of biotin-BSA (0.5 mg/mL in 0.1 M sodium bicarbonate, pH 8.6; Sigma Aldrich, Germany), overnight at 37°C in a humidified incubator. The cantilevers were washed three times in PBS (phosphate buffered saline) pH 7.4 to remove unbound protein. After that the cantilevers were incubated to a 50µl drop of streptavidin (0.5 mg/mL in 0.01 M PBS, pH 7.4) for 30 min at room temperature. The cantilevers were washed 3 times in PBS,

and finally, the cantilevers were incubated in biotin-concanavalin A solution (0.4 mg/mL in PBS, Sigma Aldrich, Germany) for 30 minutes at room temperature (*vd.* Figure III.1).

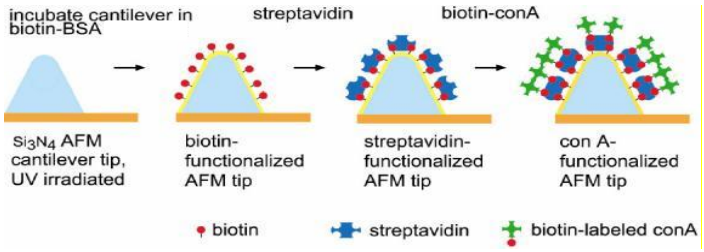

Figure III.1 - Functionalization of an AFM tip with concanavalin A. Unsharpened Si_3N_4 AFM cantilevers were functionalized with biotinylated bovine serum albumin (biotin-BSA) coupled with avidin bound to biotinylated con A. Figure from (Wojcikiewicz *et al.*, 2004).

Single cells were captured by positioning the con A-functionalized cantilever above the cell centre and gently lowering onto the cell for, approximately, 30 seconds. The settings were appropriately optimised. The applied force was adjusted to 0.3 nN before retraction. Data collection for each force-distance cycle was performed at 3 µm/s and with a z-length of 30 µm. A retract delay and an extend delay of 5 seconds were applied. We measured the adhesion force in different fibrinogen concentrations (from 0 mg/ml to 1.0 mg/ml of fibrinogen) (Sigma Aldrich, USA) for control and patients. For each blood sample, approximately, 40 force *vs.* distance curves were performed for each concentration (5 curves × 8 cells attached in a poli-L-lysine glass slides). The incubation with fibrinogen was during 15 minutes for each protein concentration tested (0.0, 0.4 and 1.0 mg/mL) before the measurements have been performed. Well-defined and measurable adhesion forces curves were observed for the interaction between erythrocyte-erythrocyte in the presence and in the absence of fibrinogen molecules. Force-distance curves were analysed using JPK Image Processing software v.5.1.8 (JPK Instruments, Berlin, Germany).

5) *Haemorheological Parameters*

Rheology is a specialized part of fluid mechanics and is concerned mainly with non-Newtonian and viscoelastic substances. A non-Newtonian liquid is one in which the viscosity depends on shear stress. The phase blood rheology implies that blood exhibits a variable viscosity depending on how rapidly it is forced to flow under shear (Kaibara, 1996).

A non-Newtonian rheology of blood is considered on the interaction of fibrinogen with erythrocytes. At normal haematocrit levels, no other plasma protein in the absence of fibrinogen seems capable of producing a yield shear stress in erythrocytes (Kaibara, 1996).

The blood rheological properties are the basic science and clinical interest. Blood is considered a non-Newtonian suspension containing cells (*e.g.*, erythrocytes, leukocytes and platelets), lipid components, proteins, carbohydrates and electrolytes. Blood flow is characterized by several haemorheological parameters and the concentration of cellular elements in blood and their rheological properties are important determinants of blood fluidity (Santos *et al.*, 2011). Normal erythrocytes are highly

deformable bodies and tend to orient themselves with the flow streamlines, especially if the shear forces are high enough to slightly deform these cells. Erythrocyte deformation and orientation are the primary cellular factors affecting blood viscosity at high shear rates (Baskurt & Meiselman, 2003). Various epidemiological studies indicated a possible relationship between blood rheology and coronary heart disease incidence (Sargento *et al.*, 2003; Guedes *et al.*, 2016). To study haemorheology it is important to know the characteristics of various types of blood vessels. The arterial system consists of aorta, arteries, arterioles, terminal arterioles and capillaries. All vessels have different diameter, wall thickness and others characteristics. The venous system consists of veins, vena cava, venues and others vessels. As the arterial system, the venous system has different diameter, wall thickness and others characteristics. This information can be seen in Figure III.2.

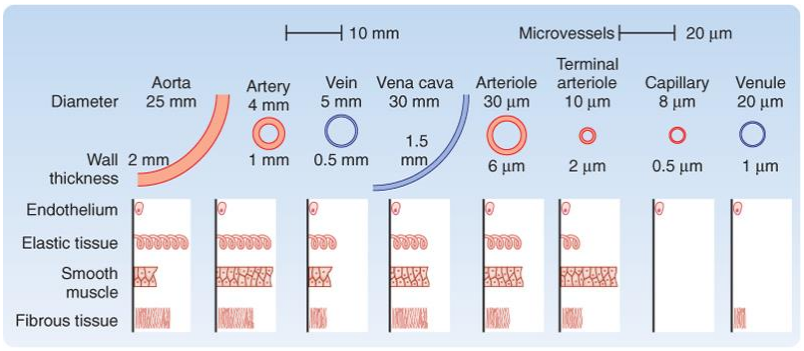

Figure III.2 - Characteristics of various types of blood vessels in humans, mainly in arterial and venous system. (Figure from https://s-media-cache-ak0.pinimg.com/236x/07/67/f4/0767f4ccaa40677fbe4975d3aac63ab1.jpg).

Haemorheological parameters are influenced by all blood cells and blood compounds. On this study, the human blood was collected into heparin anticoagulant tubes, and erythrocyte deformability, erythrocyte aggregation and whole blood viscosity were determined.

5.1) Erythrocyte Deformability

Introduction of the method

Erythrocytes transports oxygen and they need to traverse the capillaries of the microvascular system with internal diameters of 4-5 µm. In normal conditions, the erythrocytes deform sufficiently to across these narrow passages. The cellular deformability, defined as the ability of a cell to adopt a new shape in response to deforming forces, is essential for microvascular tissue perfusion (Rabai *et al.*, 2014). Erythrocyte deformability can be modified by several structural and functional alterations of erythrocytes generated by genetic or environmental factors. It is known that the reduction in erythrocyte deformability under certain physiological or pathological conditions results into the retardation of blood-flow through the microcirculation. The erythrocytes are extremely deformable because they can progressively elongate under shear stress. At higher shear stress, the erythrocytes respond by elongating itself in capillaries. So they are capable of entering and transiting in blood vases with smaller diameters. When the cells deform their surface area remains fixed. The erythrocyte

membrane resists to the dilation of its area and only ruptures above 2-3% of its area expansion (Santos *et al.*, 2011).

The unique shape and structure of erythrocytes confer special mechanical properties to them. Erythrocytes behave as elastic bodies, and thus the shape change is reversible when the deforming forces are removed. Erythrocytes also exhibit viscous behaviour and respond as a viscoelastic body. The erythrocytes membrane can exhibit plastic changes under some pathological circumstances and can be permanently deformed by excessive shear forces (Baskurt & Meiselman, 2003). The membrane elastic and cytoplasmic viscosity properties are determinant factor for erythrocyte deformability. Erythrocyte deformability can be quantified by monitoring changes in cell shape after applying fluid forces (Baskurt & Meiselman, 2003). In healthy conditions erythrocytes can pass capillaries with diameters smaller than their cell size, but if clotting occurs, the blood flow might stop. In the case of wound healing, clotting is life-saving, but in a healthy vessel a thrombus might lead to a stroke. Pathophysiological processes can result in reversible or irreversible deterioration of erythrocyte rheological behaviour (Baskurt & Meiselman, 2003).

Sample preparation/measurement

Erythrocyte deformability can be studied by ektacytometry. This technique simulates the fluid flow and the vessel wall conditions, in which a laser beam is projected through a dilute erythrocyte suspension and the resulting diffraction pattern analysed to determine erythrocyte shape and hence a deformation index, also known as an elongation index. The erythrocyte deformability is semi-quantitatively evaluated (Martins e Silva & Saldanha, 2005).

For our erythrocyte deformability measurements, the human whole blood was collected into heparin anticoagulant tubes and suspended with Dextran 40,000 buffer in isotonic NaCl solution (low viscosity), in a final concentration of the suspension 1.5% (v/v). The erythrocyte deformability was determined using a shear stress diffractometer (Rheodyne SSD laser diffractometer, Myrenne, Roetgen, Germany) at 0.3, 0.6, 1.2, 3.0, 6.0, 12.0, 30.0 and 60.0 Pa shear stress values. These values mimic the values of shear stress in blood vases in physiological conditions.

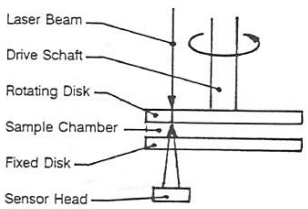

Figure III.3 - Principle of erythrocyte deformability technique. In sample chamber is inserted the erythrocyte solution with elevated viscosity between two discs. Upper disk is a rotating optical glass and the fixed disk is a stationary polymethacrylate. The diffraction pattern is circular with erythrocytes. A laser beam is allowed to pass through the erythrocyte suspension and a diffraction pattern appears. These light intensities are measured along two axes, and the relative "Elongation Index" is obtained. The measurement is performed by applying different types of shear stress values in the blood sample. Figure from (Martins e Silva & Saldanha, 2005).

5.2) Erythrocyte Aggregation

Introduction of the method

Erythrocytes aggregation is also one the most important factors affecting the blood flow. The increased erythrocyte aggregation is a cardiovascular risk factor, associated with others clinical conditions, such hypertension and hypercholesterolemia. Erythrocytes hyperaggregation occurs in diabetes, atherosclerosis, arterial hypertension, ischaemic heart disease, stroke and others vascular pathologies (De Oliveira *et al.*, 2012). "Pathologic aggregates" are known to occur also in myocardial infarction, nephrotic syndrome and after prolonged storage of blood samples (Baskurt & Meiselman, 2003).

Erythrocyte aggregation occurs when biconcave discoid cells "stick" face-to-face to form the so-called "rouleaux" at sufficiently-low shear forces (Baskurt & Meiselman, 2003, 2007). Erythrocyte aggregation is also dependent on the local shear forces, as the aggregates are reversible and easily broken into smaller aggregates (or individual cells) under increasing shear forces. An important consequence of this shear-dependent nature of erythrocyte aggregation is the non-newtonian behaviour of blood. Blood viscosity increases with increase number of erythrocyte aggregates, holding more cells into three-dimensional rouleaux under low-shear conditions (Baskurt & Meiselman, 2003, 2007).

Erythrocyte aggregation is a major determinant of the *in vitro* rheological properties of blood (Neu *et al.*, 2008). It is known that an increase of fibrinogen concentration and of erythrocyte aggregation are significant risk factors during various cardiovascular and cerebrovascular diseases (Lominadze & Dean, 2002). Erythrocyte aggregation can be influence by biochemical, haemorheological and haemodynamic factors. At low shear rates observed at venous system an increase in erythrocyte aggregation induce an increase in blood viscosity and consequently impaired blood velocity (Saldanha, 2002). The mechanism of erythrocyte aggregation is that it results from an increase in plasma adhesion proteins such as fibrinogen (Lominadze & Dean, 2002). Fibrinogen and others plasma proteins promote erythrocyte aggregation, with aggregation dependent on the magnitude of shearing forces acting on the cells (Baskurt & Meiselman, 2003).

There are two models proposed for erythrocyte aggregation: (i) the "Bridging model" that bridging forces due to the adsorption of macromolecules onto adjacent cell surfaces exceed disaggregating forces; and (ii) the "Depletion model" that result of a lower localized protein or polymer concentration near the cell surface compared to the suspending medium. Disaggregation forces are electrostatic repulsion, membrane strain, and mechanical shearing (Neu *et al.*, 2008).

Sample preparation/measurement

Blood cells suspension were prepared with different fibrinogen (fraction I, type I, human plasma, Sigma, ref. F-3879) concentration (0, 20, 40, 60, 80 mg/dL) into NaCl 0.9% that were added to 500 µL

of human blood. Blood was collected into heparin anticoagulant tube. The suspensions were incubated for 30 minutes, in room temperature. The erythrocyte aggregation was measured in a Myrenne aggregometer (model MA-1, Myrenne GmbH, Roetgen, Germany). The system measures the infrared light transmission through an erythrocyte suspension between a transparent plate and a cone, at stasis during 5 s and 10 s after dispersion of the blood samples, or rotation at shear stress of 600 s^{-1} (Santos *et al.*, 2011).

5.3) Whole Blood Viscosity

Introduction of the method

Blood and plasma viscosity are one of the major factors affecting blood flow and normal circulation. Whole blood viscosity is chiefly affected by plasma viscosity, erythrocyte deformability, haematocrit, and other physiological factors. Increase in the blood viscosity was associated with the development of multiple disorders via damaging the vascular endothelium. It also has a correlation between blood viscosity and cerebrovascular disorders (Alkuraishy *et al.*, 2014). Plasma viscosity depends of the concentration of plasma proteins, and it has Newtonian fluid properties. Plasma viscosity was considered as a marker of acute disease due to elevation of plasma proteins mainly fibrinogen (Alkuraishy *et al.*, 2014). Blood viscosity is higher in patients with cerebrovascular disorders due to higher haematocrit, and this is correlated with infarct size and increase of the risk of mortality (Alkuraishy *et al.*, 2014). Increase in the blood viscosity induces endothelial damage, inflammation, vascular wall hypertrophy, platelet aggregation and deterioration in the blood vessels shear stress. All these factors increase the risk of a stroke and cardiac ischemia events. Blood viscosity is usually higher at the morning. This circadian rhythm is due to higher fibrinogen level at morning which explained the higher rate of stroke during that time (Alkuraishy *et al.*, 2014). Gender differences in blood viscosity is related to the erythrocytes rigidity and aging. The degree of disturbance of flow streamlines and consequently the viscosity of blood is thus strongly dependent on the haematocrit. There are major dissimilarities among males and young females at reproductive period in whole blood viscosity. Different studies previously showed that high haematocrit and blood viscosity were significantly correlated with male cerebrovascular disorders (Alkuraishy *et al.*, 2014). Because of the female menstruations there are significant gender differences in all viscosity parameters, as for the decrease of haematocrit leading to lower blood viscosity in female. Approximately 0.8% of total red blood cells reformed per day, and 80% of female erythrocytes were younger (Alkuraishy *et al.*, 2014). Thus, the viscosity of the blood depends on the viscosity of the plasma in combination with the haematocrit. Higher haematocrit implies higher viscosity (Westerhof *et al.*, 2005). For normal blood at 37°C, blood viscosity at high shear rate (100~200 s^{-1}) is measured as 4 ~ 5 cP (Kim *et al.*, 2012).

Sample preparation/measurement

Whole blood viscosity was evaluated in a Brookfield digital viscometer (Brookfield, USA). For that it was used native whole blood collected into heparin anticoagulant tube, submitted to low (22.5 s^{-1}) and high (225 s^{-1}) shear rates, both at a native and after correction of the haematocrit of 45%, and at 37ºC. Viscosity of a liquid depends on its temperature, so the viscosity of blood is usually measured at constant temperature by a rotational viscometer. Several units have been used for viscosity, with the most common being milliPascal.sec (mPa.s) which is numerically equal to centipoise (cP). The blood in the human circulatory system is affected by wide variations in shear rate and the viscosity measurements can be variable in 6.0 to 8.0 mPa.s at low shear rate and 4.4 to 5.2 mPa.s at high shear rate (Martins e Silva & Saldanha, 2005; Santos *et al.*, 2011; Guedes *et al.*, 2016).

6) *Fibrinogen Quantification*

6.1) Total Plasma Fibrinogen Quantification

Increased levels of plasma fibrinogen result in changes in blood rheological properties, and these alterations exacerbate the complications in peripheral blood circulation during cardiovascular pathologies. Thus, it is important to quantify the fibrinogen levels in human plasma. For fibrinogen quantification, the blood was collected into sodium citrate anticoagulant tube. In a centrifuge (Sorvall TC6), blood was centrifuged at 3000 rpm for 10 min. The plasma was collected for the fibrinogen quantification measurement which was performed in Dade Behring BFT II Coagulation Analyzer (Behring, Germany).

The coagulation analyser is a semi-automated, dual-channel coagulometer, and its permit the fibrinogen quantification in mg/dL Used a temperature-controlled incubation block for reagents (Multifibren*U, Siemens) and samples, at 37ºC (*vd.* Figure III.4). The Multifibren*U method is a modification of the Clauss method, a functional assay based upon the time for fibrin clot formation, where the citrated plasma is brought to coagulation by a large excess of thrombin. Here the coagulation time depends largely on the fibrinogen content of the specimen (Siemens Healthcare Diagnostics Products, 2008).

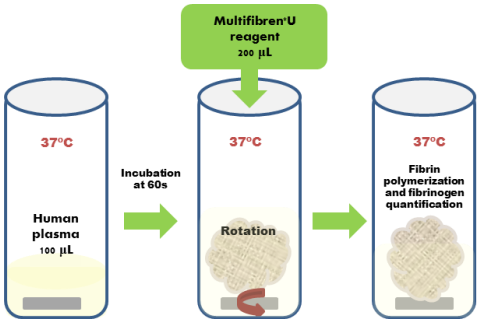

Figure III.4 - Process of total plasma fibrinogen quantification using the Multifibren*U method.

6.2) γ' Fibrinogen Quantification

For the quantification of γ' fibrinogen, it was done an assay that is intended to be used as part of a risk for cardiovascular disease assessment in adults. In a centrifuge (Sorvall TC6), blood collected into sodium citrate anticoagulant tube is centrifuged at 3000 rpm for 10 min. The γ' fibrinogen assay uses human venous plasma samples. It is a semi-automated quantitative ELISA method that consists in a two-site sandwich immunoassay by Gamma Coeur Test Kit (Gamma Therapeutics, Inc., Portland, Oregon). γ' fibrinogen in the sample binds to a specific monoclonal antibody for this protein which was coated on the 96-microwells plate (*vd.* Figure III.5). Every sample was done in duplicated. After incubation, unbounds non- γ' fibrinogen, such as γAγA fibrinogen, and others plasma components (*vd.* Figure III.5B) were removed by sequential washing. Horse radish peroxidase (HRP)-labeled polyclonal secondary antibody was added, which binds to the captured γ' fibrinogen, forming a "capture antibody/analyte/detection antibody" sandwich (*vd.* Figure III.5D). After this, excess detection antibody was removed by several sequential washings and a substrate for the HRP-labeled detector was added to generate a coloured product (*vd.* Figure III.5E). After the secondary antibody, a solution to stop the reaction was added to each well and the absorbance of the yellow coloured end product was read on a spectrophotometer at 450 nm. The average of each set of duplicates was calculated for each samples (healthy donors, stroke and ALS patients) and the results from the standards were confirmed (Mannila *et al.*, 2007; Lovely *et al.*, 2010; Farrell, 2014). Eight solutions of γ' fibrinogen with increased fibrinogen concentrations were used as calibrators of a standard calibration curve (Farrell, 2014).

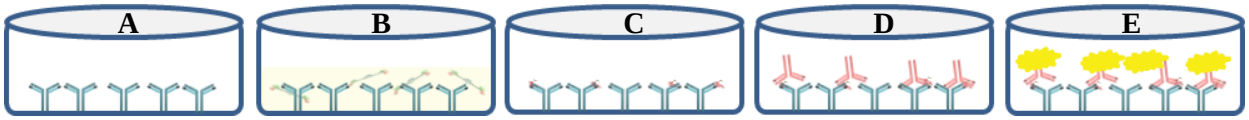

Figure III.5 - Process of the γ' fibrinogen quantification by ELISA method.

7) *Zeta-Potential*

7.1) Introduction of the method

Most liquids contain ions, and a charged particle is suspended in a solution of an opposite charge will be attracted to the surface of the suspended particle (Malvern Instruments, 2004). The liquid layer surrounding the particle exists as two parts, an inner region, where the ions are strongly bound, that is commonly called the stern layer. The stern layer has composed by positive ions that are called counter-ions. The attraction from the negative charged membrane surface causes some of the positive ions to form a firmly attached layer. The second layer is the diffuse layer, where ions diffuse more freely, less firmly associated and is composed by negative and positive ions. This causes a dynamic equilibrium because the positive ions are still attracted by negative colloid but they are repelled by the stern layer (*vd.* Figure III.6) (Freire *et al.*, 2011; Malvern Instruments, 2011).

A potential exists between the particle surface and the dispersing liquid which varies according to the distance from the particle surface is the zeta-potential (ζ-potential) (Malvern Instruments, 2004). Zeta-potential is a physical property which is exhibited by any particle in suspension (Malvern Instruments, 2011) and this is calculated based on the electrophoretic mobility of the particles in solution, on an electric field, to the electrode of opposite charge (Domingues *et al.*, 2008; Freire *et al.*, 2011).

The ζ-potential is used as a combination of two measurement techniques: electrophoresis and Laser Doppler velocimetry. The electrophoretic mobility of the scattering particles in a sample can be calculated essentially by Laser Doppler velocimetry (Malvern Instruments, 2004). Laser Doppler velocimetry is a technique that relates the frequency measured by intensity fluctuation of the scattered light. The sensitivity of the Doppler Effect to the low mobility of larger particles is very low, causing difficulties in calculating the electrophoretic mobility (Domingues *et al.*, 2008; Freire *et al.*, 2011).

The zetasizer Nano Series calculates the ζ-potential by determining the electrophoretic mobility and then applying the Henry equation. The development of a net charge at the particle surface affects the distribution of ions in the surrounding interfacial region. The magnitude of the ζ-potential gives an indication of the potential stability of the colloidal system.

The Henry equation is defined by:

$$\zeta = \frac{3\eta u}{2\varepsilon f(ka)} \qquad (2)$$

Where η is the viscosity of the solvent, u is the electrophoretic mobility, ε is the dielectric constant and $f(ka)$ is the Henry's function. The value of this function is considered to be 1.5 when the particles are suspended in aqueous solutions with high ionic strength (Smoluchowski's approximation, that fits well to physiological conditions), and 1 when non-aqueous media are used (Huckel approximation). Using this simple approach the surface charge potential of molecules in solution and the change in this parameter, as a result of interactions with biologically relevant ligands, can be easily

monitored. Thus, allowing the determination of the role of charges in biological interactions. The ζ-potential of a particle is proportional to its surface charge (Domingues *et al.*, 2008).

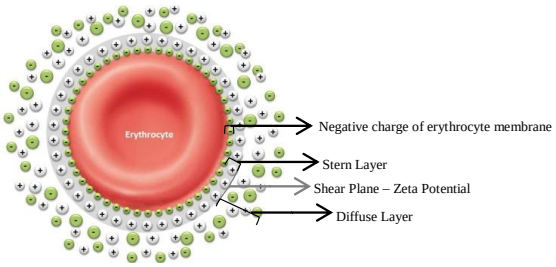

Figure III.6 - Composition of erythrocyte and zeta-potential of their surface membrane. The erythrocyte has a negatively charged surface membrane and this causes some of the positive ions to form a firmly attached layer. The ions have strongly bound to particle (Stern layer). The diffuse layer, where ions diffuse more freely is composed by negative and positive ions. A potential exists between the particle surface and the dispersing liquid which varies according to the distance from the particle surface, is the Zeta-Potential (ζ-potential) (Malvern Instruments, 2004).

7.2) Samples preparation and measurement

Human blood was collected into K_3EDTA anticoagulant tube and erythrocytes were isolated according the already described procedure. BSGC with $CaCl_2$ buffer at pH 7.3 were filtered using a syringe filter with 0.45 µm pore size (Whatman, Florham Park, NJ) to remove any large scattering particle, which would bias the light scattering measurements. The erythrocytes suspension was set to 0.035% of haematocrit in BSGC with $CaCl_2$ buffer pH 7.3, in the absence or in the presence of different soluble human variants fibrinogen concentrations (0.0-2.0 mg/mL). With a 1 mL syringe, the sample was injected into the folded capillary cell (DTS 1060) (Malvern, UK) (*vd.* Figure III.7).

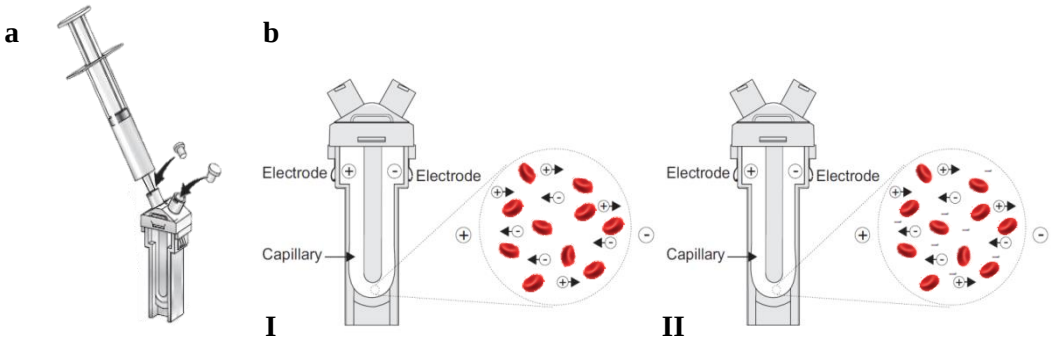

Figure III.7 - Process for inserting the sample into the folded capillary cell **(a)**. Scheme of the Zeta-Potential: with the erythrocytes suspension (I), and erythrocytes suspension with fibrinogen molecules (II) **(b)**. Images adapted from (Malvern Instruments, 2004).

On this project, it was used a software to control the measurement of the sample. SOP measurements can be pre-defined the settings for all the measurement. Zeta-potential analysis were performed as described by Carvalho *et al.*(2011). Measurements were conducted on a ζ-potential equipment Malvern Zetasizer Nano ZS (Malvern, UK), equipped with a He-Ne laser (λ=632.8 nm). The ζ-potential of the samples were determined, at 25ºC, from the mean of 15 measurements, with 60 runs each, with an applied potential of 30V, in absence and presence of different soluble human fibrinogen concentrations (0.4 at 2.0 mg/mL), using a specific cuvette (Carvalho *et al.*, 2011). Before the measurements, the samples were allowed to pre-incubate for 10 minutes.

8) *Fluorescence Generalized Polarization*

8.1) Introduction of the method

The rheological properties, and other cellular functions, such as permeability and mobility, are regulated by membrane fluidity. An approach of fluidity can be made by using fluorescence polarization with fluorescent probes distributed in the lipid areas of membranes (Donner & Stoltz, 1985). On this study was used laurdan (2-dimethylamino-6-lauroylnaphthalene), that is a polarity sensitive probe. Laurdan was designed and synthesized by Gregorio Weber, to study the phenomenon of dipolar relaxation. It is a naphthalene derivative, which is used as a fluorescent dye when applied to fluorescence microscopy (Sanchez *et al.,* 2012). The fluorescent naphthalene moiety of these probes has a dipole moment due to a partial charge separation between the 2-dimethylamino and the 6-carbonyl residues. This dipole moment increases upon excitation and may cause reorientation of the solvent dipoles. The bilayer fluidity-dependent fluorescence spectral shift of laurdan can have dipolar relaxation phenomena. Upon excitation, the dipole moment of laurdan increases noticeably and water molecules in the proximity of the probe reorient around this new dipole. When the membrane is in a fluid phase, the reorientation rate is faster than the emission process and, consequently, a red-shift is observed in the emission spectrum of laurdan. When the bilayer packing increases part of the water molecules is excluded from the bilayer and the dipolar relaxation of the remaining water molecules is slower, leading to a fluorescent spectrum which is significantly less shifted to the red (Domenech *et al.,* 2010). The emission spectrum of laurdan within a single phospholipid bilayer is centered at 490 nm when the lipids are in a disordered phase and is shifted to the blue (around 440 nm) when the lipids are in a more packed phase (Sanchez *et al.*, 2012). Changes in lipid fluidity can sometimes be related with either pathological processes or membrane alterations caused by cell interactions with exogenous molecules. It is therefore important that the indications obtained regarding lipid fluidity should be accurately correlated with membrane structure or functions. However, biological membranes represent very heterogeneous media and the use of probes which label different compartments of cell membranes is required to get a better knowledge of membrane fluidity. Polarity changes are detected by shifts in the laurdan emission spectrum, and the Generalized Polarization function (GP) was defined as a way of measuring wavelength displacements. Changes in GP values when lipid bilayers are either in fluid or gel phase extended the use of the technique to the field of membrane dynamics and protein interaction (Sanchez *et al.*, 2012). The concentration and molecular dynamics of the water molecules is a function of the phospholipid phase state, where water reorientation along the probe excited-state dipole occurs only in the liquid-crystalline phase. The Generalized Polarization (GP) function is defined as:

$$GP = \frac{I_{440} - I_{490}}{I_{440} + I_{490}} \quad (3)$$

where I_{440} and I_{490} are the emission intensities at 440 and 490 nm respectively. It is used to investigate membrane qualities of the phospholipid bilayers of cell membranes. The hydrophobic tail of the lauric fatty acid allows solubilisation of the probe within phospholipid bilayers, locating the fluorescent moiety toward the aqueous environment. When laurdan get the phospholipid bilayers, it can be seen in Figure III.8 some water molecules penetrating the lipid bilayer (Yu *et al.*, 1996).

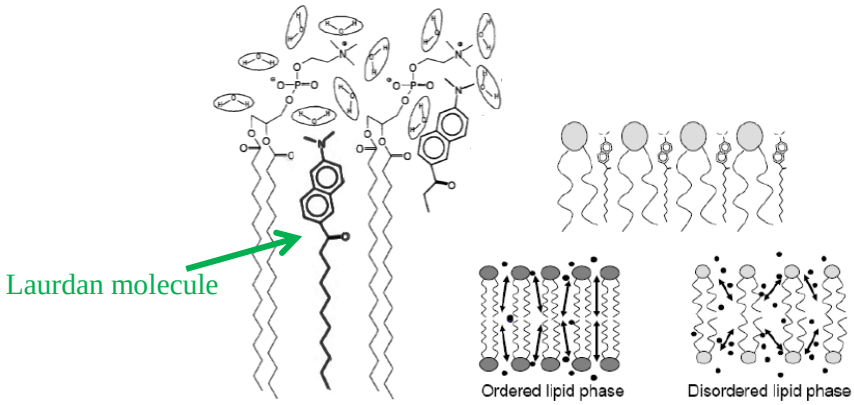

Figure III.8 - Scheme of laurdan anchored into phospholipid bilayers in presence of some water molecules and localized in ordered lipid phase and disordered lipid phase. Adapted from (Parasassi *et al.*, 1998; Harris *et al.*, 2002).

In phospholipid bilayers laurdan is tightly anchored in the hydrophobic core by the cooperative van der Waals interactions between the lauric acid tail and the lipid hydrocarbon chains, with its fluorescent moiety residing at the level of the phospholipid glycerol backbone (Parasassi *et al.*, 1998). Cuvette measurements of laurdan GP are done in a conventional fluorometer using excitation light at 340-360 nm and by simply registering the two mentioned emission intensities (Sanchez *et al.*, 2007).

8.2) Samples Preparation and Measurement

Human venous blood samples were collected into heparin anticoagulant tube from healthy donors and ALS patients. Whole blood samples were centrifuged for 5 min at 3000 rpm in Sorvall TC6 centrifuge (Du Pont, Bad Naughem, Germany). Erythrocytes were isolated according the procedures mentioned before. The erythrocytes suspension was set to 0.037% of haematocrit in phosphate buffer 155mM, pH 7.4. The erythrocyte suspension was incubated for 30 min, at room temperature, in absence (baseline) and in the presence of fluorescent probe laurdan, with the total final concentration of 3.59 µM. Laurdan was dissolved in DMSO (di-methyl sulphoxide). The Fluorescence Generalized was measured on a Varian Cary Eclipse fluorescence spectrophotometer (Mulgrave, Australia). The measurements were done with λ_{exc}=350 nm, and acquiring the full spectra between 400 nm and 600 nm. Typical spectral bandwidths were 5 nm for excitation and 10 nm for emission. Excitation and emission spectra were corrected for wavelength-dependent instrumental factors. After the measurements, it was necessary to normalize the spectra for the maximum, and to calculate the Generalized Polarization of the samples.

9) *Statistical Analysis*

For each parameter, both groups of the patients (stroke and ALS patients) were compared with the control group of healthy donors. The statistical intergroup comparison was performed by applying the unpaired Student's t test. Data are shown as mean value ± standard error of the mean (S.E.M.). Statistical significance was valued for values of $p<0.05$ with 95% of confidence interval. Statistical analyses were performed using GraphPad Prism 5.03.

IV) Results and Discussion

1) Results with Stroke patients

At the time of the writing of this thesis it was impossible for us to obtain the clinical data of each stroke patient included on the project.

The erythrocyte deformability was determined by exposing the cell to different shear stress values that vary between 0.3 and 60.0 Pa. These values represent the shear stress inside blood vessels of different diameters in physiological process. The results are presented in Figure IV.1. It can be seen that, at low shear stress, which represent the larger diameter vessels, the erythrocytes from stroke patients are more deformable than erythrocytes from control (* p=0.0234 at 0.3 Pa, ** p=0.0039 at 0.6 Pa, * p=0.0430 at 1.2 Pa). In smaller diameter vessels, at high shear stress the erythrocytes from stroke patients has lower deformability than erythrocytes from control (* p=0.0424 at 12.0 Pa).

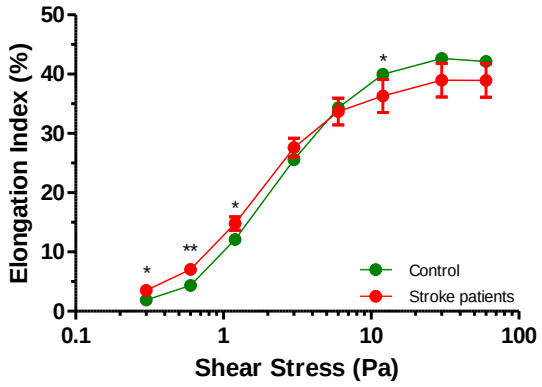

Figure IV.1 - Erythrocyte deformability measured at different shear stress values for stroke patients (n=6) and control group (n=57). Values are presented as mean ±SEM. At low shear stress, that represent the higher diameter vessels, the erythrocytes from stroke patients' are more deformable than erythrocytes from control (* p=0.0234 at 0.3 Pa, ** p=0.0039 at 0.6 Pa, * p=0.0430 at 1.2 Pa). With the increased of the shear stress, lower diameter vessels promote an increase of erythrocyte deformability, but in smaller diameter vessels, at high shear stress the erythrocytes from stroke patients are less deformable than erythrocytes from control (* p=0.0424 at 12.0 Pa).

The results from erythrocyte aggregation are detailed, in Figure IV.2. The erythrocyte aggregation was measured by the infrared light transmission through a whole blood suspension, at stasis during 5 seconds (*vd.* Figure IV.2a) and 10 seconds (*vd.* Figure IV.2b), with the addition of different fibrinogen concentrations (0.0 to 80.0 mg/dL). It could be observed that without addition of fibrinogen, at 5 and 10 seconds, the erythrocytes from stroke patients had a lower tendency to aggregate than the control. Erythrocyte aggregation increased with increasing of fibrinogen concentration in control samples. In stroke patients the dependence of the addition of fibrinogen concentration is not evident. The erythrocyte aggregation in stroke patients measured at 5 seconds (*vd.* Figure IV.2a) and 10 seconds (*vd.* Figure IV.2b) in presence of fibrinogen 20.0 mg/dL, is higher than the control. Although, these difference were not statistically significant. In blood samples from stroke patients it appears that there

is a saturation of fibrinogen molecules on plasma which leads to a plateau of erythrocyte aggregation index values.

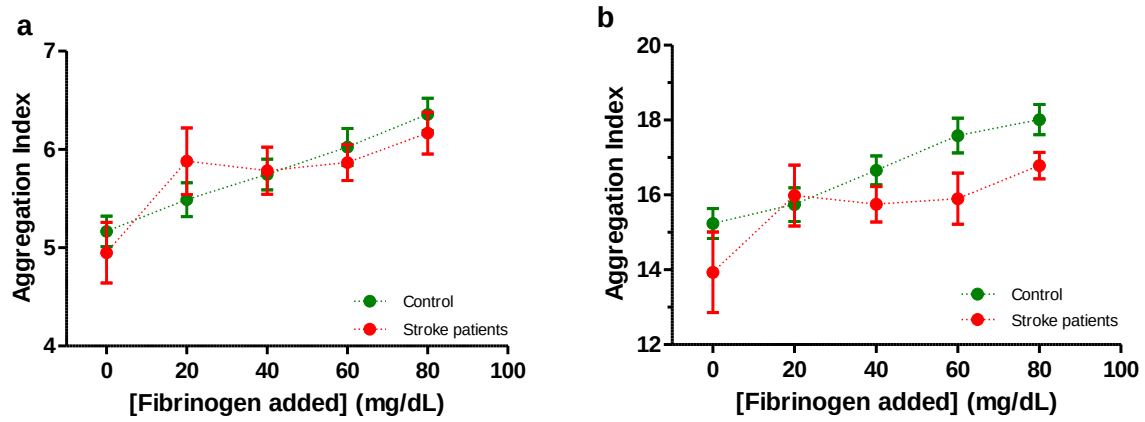

Figure IV.2 - Erythrocyte aggregation measured in function of the addition of fibrinogen on blood from stroke patients (n=6) and control group (n=57) with addition of the different concentrations of fibrinogen (0.0 to 80.0 mg/dL). The erythrocyte aggregation was measured during 5 seconds **(a)** and 10 seconds **(b)**. Values are presented as mean±SEM.

Figure IV.3 shows the results of the whole blood viscosity, measured in blood from stroke patients and control at low (22.5 s^{-1}) and high (225 s^{-1}) shear rates, both at a native (*vd.* Figure IV3a,b,c) and corrected samples with haematocrit of 45% (*vd.* Figure IV.3d, e, f), at 37ºC. The applied shear rate and the diameter of the vessels are inversely proportional mimicking the physiological process. An increase of the shear rate, promotes a decrease of the viscosity of the blood being this related with smaller diameter vessels (*vd.* Figure IV.3c, f). On the other hand, at low shear rate, there was an increase of the viscosity, and this occurs in higher diameter vessels (*vd.* Figure IV.3c, f). At all shear rates, both the groups have not statistically significant differences on their whole blood viscosity values. But, it is possible to see that stroke patients have a tendency for higher values of viscosity than the control. At low shear rate the control values of viscosity was of 7.25±0.17 mPa.s *vs*. 7.68±0.11 mPa.s from stroke patients (*vd.* Figure IV.3a). For whole blood viscosity with haematocrit at 45% the control group has 7.22±0.08 mPa.s *vs.* 7.64±0.45 mPa.s from stroke patients (*vd.* Figure IV.3d). At high shear rate (*vd.* Figure IV.3b, e), it is observed that the control for native blood viscosity showed a tendency for lower viscosity than the stroke patients (4.40±0.08 mPa.s *vs*. 4.70±0.14 mPa.s). For haematocrit at 45% at high shear rate the same tendency was observed (4.51±0.05 mPa.s *vs.* 4.66±0.11 mPa.s). All the comparisons of results from control and stroke patients were not statistically significant.

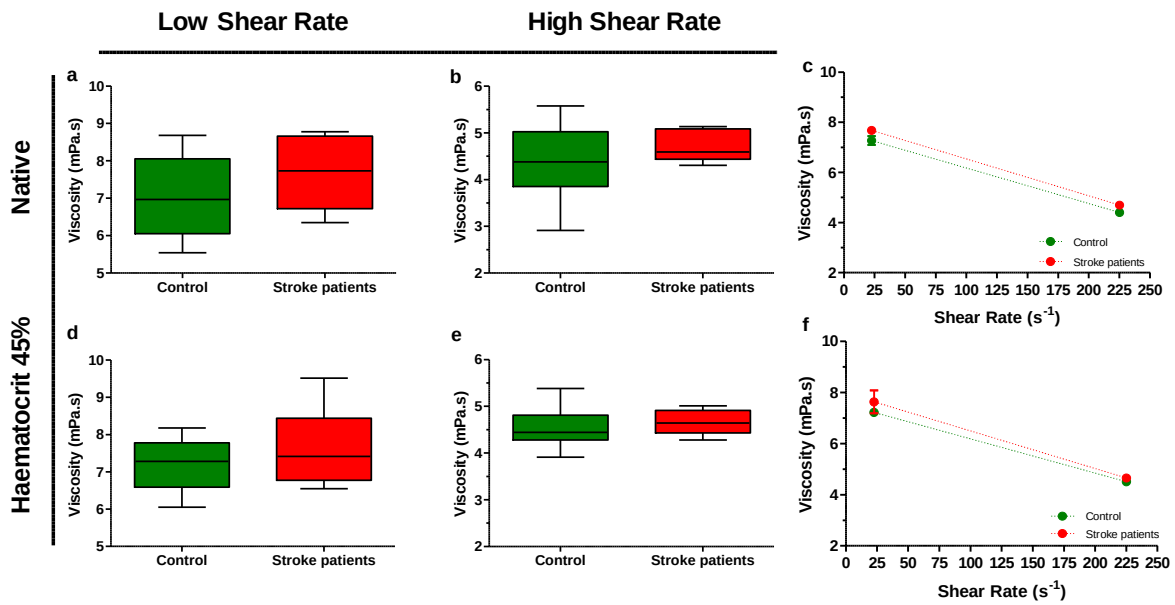

Figure IV.3 - Variations on whole blood viscosity between stroke patients and control. The whole blood viscosity was measured in blood from stroke patients (n=6) and control (n=57) at low (22.5 s^{-1}) and high (225 s^{-1}) shear rates, both at a native **(a, b, c)** and corrected samples with haematocrit of 45% **(d, e, f)**, at 37ºC. Values are presented as box with median and whiskers with maximum and minimum values **(a,b,d,e)** and mean±SEM **(c,f)**.

Total fibrinogen levels were quantified on stroke patients and control group (*vd*. Figure IV.4a). Increasing plasma fibrinogen levels can result in changes in blood rheological properties, and these alterations exacerbate the complications in peripheral blood circulation during cardiovascular pathologies. The normal range of the total fibrinogen concentration on the plasma is 180 to 350 mg/dL and elevated fibrinogen levels have been associated with a risk factor for cardiovascular disease. Thus, it can be seen that stroke patients have high fibrinogen concentration in plasma than the control group (290.7±19.31 mg/dL *vs*. 220.3±7.29 mg/dL, *** p=0.0007, respectively). Despite these differences between groups, both values are within the normal range of the total fibrinogen concentration levels in plasma.

γ' fibrinogen plasma levels were also quantified (*vd*. Figure IV.4b). Values that fall above the cut-off value (>30 mg/dL, represented by grey dashed line), may be indicative of increased risk of cardiovascular disease. Thus, it can be observed that stroke patients has higher concentration of γ' fibrinogen in plasma than control (54.61±7.29 mg/dL *vs*. 32.48±1.60 mg/dL, *** p<0.0001, respectively). The ratio between γ' fibrinogen and the total fibrinogen for each sample were also calculate (*vd*. Figure IV.4c). We could observed that stroke patients have more percentage of γ' fibrinogen in their plasma than the control (18.95±2.37 % *vs*. 14.83±0.70 %, * p=0.0384, respectively). As it is expected that the percentage of γ' fibrinogen in healthy conditions is approximately 15%, we could observed that stroke patients have increased risk of cardiovascular disease.

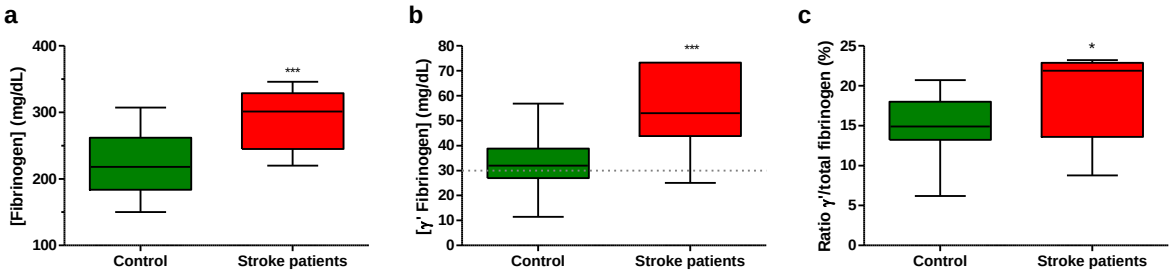

Figure IV.4 - Fibrinogen levels on plasma of stroke patients (n=6) and control (n=34)**.** Total plasma fibrinogen levels (*** p=0.0007) **(a).** γ' fibrinogen plasma quantification (*** p<0.0001) **(b)**. Ratio between γ' fibrinogen and total fibrinogen concentration present on each stroke patients and control. γ' fibrinogen levels on the plasma from stroke patients is higher than in plasma from control (* p=0.0384) **(c)**. Values are presented as box of whiskers that represent the median and maximum and minimum values.

In parallel with the other methods, erythrocyte elasticity measurements were also performed on both studied groups (*vd.* Figure IV.5). All the force spectroscopy data were analysed in order to determine the Young's modulus (*vd.* Figure IV.5a) and the penetration depth (*vd.* Figure IV.5b) for each force-distance curve. For the Young's modulus measurements, it can be seen that the erythrocytes from stroke patients are stiffer than the erythrocytes from control (3512±1440 Pa *vs*. 128.3±19.28 Pa, * p=0.0267, respectively). The Young's modulus of the erythrocytes from stroke patients is higher than control. This result is associated with the lower penetration depth of the erythrocytes from stroke patients. The penetration depth (*vd.* Figure IV.5b) was analysed by the position of the maximal movement of the piezo sensor in the z-axis. This corresponds to the z-axis coordinate when the sensor reaches an indentation force of 800 pN, subtracting the z-axis position of the sensor when the tip begins the contact with the surface of the erythrocyte. Lower penetration of the erythrocytes from stroke patients indicates that these erythrocytes are capable to deform less than those from control (526.4±1.44 nm *vs*. 811.3±7.305 nm *** p<0.0001, respectively).

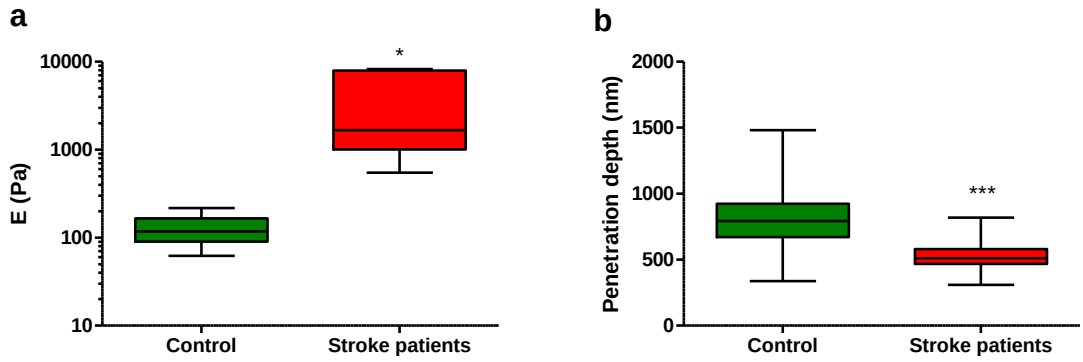

Figure IV.5 - Erythrocyte **s**tiffness measured by Atomic Force Microscopy. The stiffness or Young's modulus, of the erythrocytes from stroke patients (n=6) and control (n=7) were analysed. The values are represented as box of whiskers that represent the median and maximum and minimum values of the maximum Gaussian peaks (* p=0.0267) **(a)**. Values of penetration depth with AFM tip onto erythrocytes. The penetration depth was analysed with an indentation force of 800 pN. This parameter can measure the capacity of the erythrocytes to deform. The values are represented as box of whiskers that represent the median and maximum and minimum values (*** p<0.0001) **(b)**.

In Figure IV.6, the interaction between fibrinogen and erythrocyte membrane receptor was measured by atomic force microscopy-based force spectroscopy. In Figure IV.6a was assessed the fibrinogen-erythrocyte binding force, in picoNewton from stroke patients and control. It can be observed that the force necessary to break the interaction between fibrinogen and erythrocytes from stroke patients is higher than the control. These values were not statistically significant but it can be observed that they have different intervals of distribution. The results showed that the force necessary to break the bond between fibrinogen and erythrocytes increases from 40.42±3.00 pN in control to 67.51±20.26 pN in stroke patients (p=0.0543). We also calculate the percentage of binding frequency (%) and the results are shown in Figure IV.6b. The probability of the frequency of the binding between fibrinogen and erythrocytes was higher in control than in erythrocytes from stroke patients (27.6±4.2% *vs.* 9.23±2.76 %, * p=0.0172, respectively). Thus, in stroke patients, the force necessary to break this interaction is higher but the frequency of the binding was lower. So, in stroke, the erythrocytes can interact more with fibrinogen but less frequently.

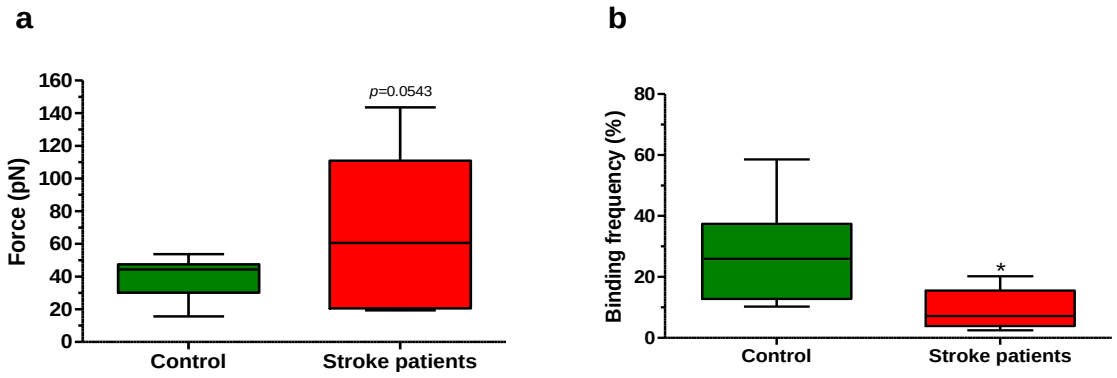

Figure IV.6 - AFM-based force spectroscopy data for the fibrinogen-erythrocyte interactions. Fibrinogen-erythrocyte binding force (pN) in erythrocyte from stroke patients and control (p=0.0543) **(a)**. Binding frequency (%) was measured by AFM in erythrocytes from stroke patients and control (* p=0.0172) **(b)**. The values are represented as box of whiskers that represent the median and maximum and minimum values.

Erythrocyte-erythrocyte adhesion studies using an AFM were also performed (*vd.* Figure IV.7). Figure IV.7a represents the work (fJ) necessary to detach two erythrocytes from each other. Without the addition of fibrinogen, when the erythrocytes interact, the work necessary to detach two erythrocytes was higher in stroke patients than the control (2.86±0.29 fJ *vs*. 0.48±0.03 fJ, *** p<0.0001, respectively). So we could conclude that erythrocyte-erythrocyte adhesion, in stroke patients, was stronger than for the control. The increase on fibrinogen concentration promotes erythrocyte-erythrocyte adhesion in erythrocytes from control. At 1.0 mg/mL of fibrinogen, the adhesion between erythrocytes from stroke patients was less strong than the control (2.38±0.22 fJ *vs*. 2.88±0.34 fJ, respectively). The detachment force (pN) was also measured in function of the addition of fibrinogen and it is shown in Figure IV.7b. The detachment force is the maxima force necessary to detach two erythrocytes. Without fibrinogen addition, the detachment force between erythrocytes from stroke patients was higher than for the control (103.0±0.03 pN *vs*. 70.20±0.23 pN, *** p<0.0001,

respectively). Identically to the values of the work (*vd*. Figure IV.7a), in detachment force when the fibrinogen concentration increases, it promotes erythrocyte-erythrocyte adhesion and this effect is more pronounced on the control. At 1.0 mg/mL of fibrinogen, the force necessary to break the interaction between the erythrocytes is higher in stroke patients than on control (152.4±0.24 pN *vs*. 137.0±0.89 pN, *** p<0.0001, respectively). Thus, with the increase of the fibrinogen concentration, the interaction between two erythrocytes was stronger in stroke patients than for the control.

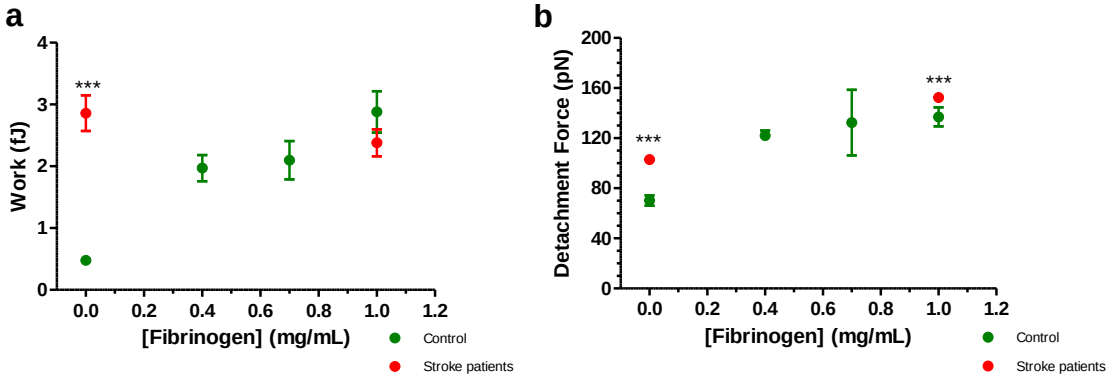

Figure IV.7 - Erythrocyte-erythrocyte adhesion study by AFM-based force spectroscopy measured in function of the different fibrinogen concentration. The work (fJ) necessary to break the adhesion between two erythrocytes from stroke patients and control, in absence and presence of fibrinogen molecules (*** p<0.0001) **(a)**. Values of detachment force (pN), in function of different fibrinogen concentrations, in erythrocytes from stroke patients and control (*** p<0.0001) **(b)**. Values are presented as mean ±SEM.

From the force-distance curve, it is possible to extract two other parameters that are important to understand the adhesion of the erythrocytes in stroke patients and control: the jumps and membrane tethers. In Figure IV.8 it is possible to observe the results from these parameters. Jumps and membrane tethers were measured on erythrocyte-erythrocyte adhesion curves in absence and presence of the fibrinogen concentrations, from stroke patients and controls (*vd.* Figure IV.8a,b)**.** The jumps events gave results about the force (pN) that occurs when the membrane of erythrocytes break the interactions between them. When the detachment occurs, the cells are separated and the bonds between ligands and receptors break. Without fibrinogen addition, the erythrocytes from stroke patients need to have stronger forces to break the interaction between them than for the control (85.42±24.75 pN *vs.* 47.78±0.31 pN, respectively). In presence of 1.0 mg/mL of fibrinogen the value of force of the jumps was lower than for the control but they were not statistically different (81.09±17.51 pN *vs.* 147.76±1.49 pN, respectively). In Figure IV.8b it is represented the values of the membrane tether forces (pN), which is other type of unbinding between membranes. Without fibrinogen, the erythrocytes from stroke patients need higher force to detach membrane tethers than control (62.12±19.68 pN *vs*. 34.98±0.10 pN, respectively). With addition of 1.0mg/mL of the fibrinogen, tethers in erythrocyte membrane from stroke patients were less strong than in erythrocyte membrane from control (83.57± 19.30 pN *vs.* 155.57± 1.21 pN, respectively).

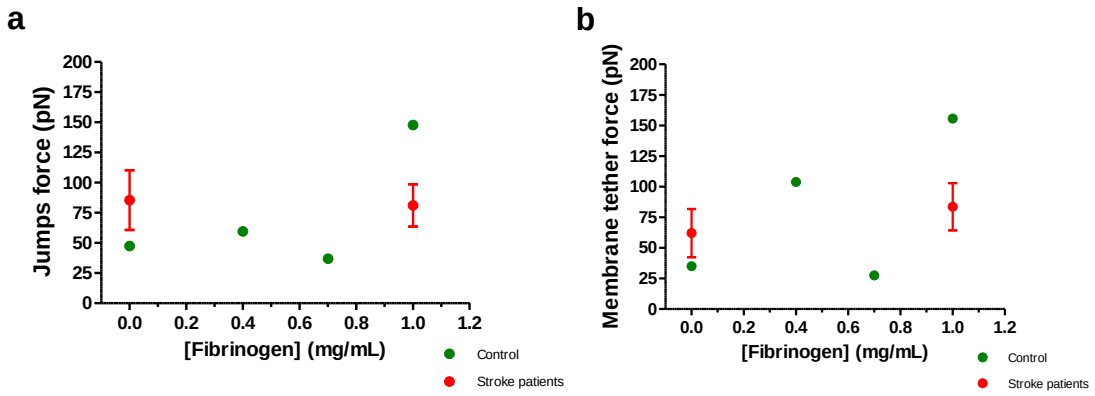

Figure IV.8 - Values of force of jumps **(a)** and membrane tethers **(b)** events formed after the binding between two erythrocytes from stroke patients and controls. Values are presented as mean ±SEM.

On this study, we used different parameters, essentiality AFM and haemorheological parameters, to better understand the interaction between fibrinogen and erythrocytes in stroke patients.

From the erythrocyte deformability technique we could conclude that erythrocytes from stroke patients are more deformable at low shear stress values, but less deformable at high shear stress values. With the increased of the shear stress, lower diameter vessels promote an increase of erythrocyte deformability. In smaller diameter vessels, at higher shear stress, the erythrocytes from stroke patients have lower deformability than erythrocytes from control. The same effect was stated by Guedes *et al.* (2016) but using erythrocytes from chronic heart failure patients, also a cardiovascular disease (Guedes *et al.*, 2016). Erythrocyte aggregation has pathogenic implications in thrombus formation. From the results we could conclude that erythrocytes from stroke patients have more tendency to aggregate. Also stroke patients have higher whole blood viscosity.

The quantification of the higher fibrinogen levels in plasma from stroke patients was also performed. This parameter has been associated with an elevated cardiovascular risk factor. Stroke patients also have higher γ' fibrinogen levels in plasma. They have an increase of the fibrinogen (total and γ' variant) quantification in plasma that is associated with high risk of cardiovascular events and could lead to a stroke event.

With AFM results, we could conclude that fibrinogen-erythrocyte interactions were modified in stroke patients.

Like in chronic heart failure disease (Guedes *et al.*, 2016), the fibrinogen-erythrocyte binding forces in stroke patients could be a potential biomarker for the risk assessment of the disease. The fibrinogen and erythrocytes interact more but with less binding frequency. The stiffness and penetration depth of the erythrocytes was also assessed and was concluded that the erythrocytes from stroke patients are stiffer and have lower penetration depth. The elasticity results confirm the results achieved with erythrocyte deformability technique.

Even without addition of the fibrinogen, from the erythrocyte-erythrocyte adhesion studies, we could conclude that stroke patients have erythrocytes with different membrane components that promote higher adhesion between them. Differences on erythrocyte membrane cytoskeleton complex are thus

expectable, promoting an increase of the changed in adhesion of the erythrocytes. In the presence of fibrinogen, the adhesion between two erythrocytes was stronger. These results indicate that fibrinogen could promote the interaction between the erythrocytes from stroke patients.

With all these results we could conclude that erythrocytes from stroke patients are less deformable, having more tendency to aggregate. Also these patients have the blood more viscous, higher levels of total fibrinogen and γ' fibrinogen in plasma and the interaction between fibrinogen and its erythrocytes are stronger. All these factors are significant risk factors for a bad prognostic of the stroke disease.

2) *Results with Amyotrophic Lateral Sclerosis patients*

The clinical profiles of the Amyotrophic Lateral Sclerosis patients studied on this thesis are summarized in **Table IV.1**. The group was settled for their demographic, clinical and laboratorial data.

Table IV.1 - The demographical and clinical parameters of ALS patients**.**

Clinical profile of ALS patients	
	ALS patients
Demographics	
No. of patients	10
Age (mean ±s.d.)	65.6 ±11.4
Male/Female (%)	70/30
Duration since disease onset (No. of patients)	
<1 year	3
1-2 years	3
>2 years	4
Onset form (No. of patients)	
Spinal	7
Bulbar	2
Respiratory	1
ALS-FRS (No. of patients)	
0-10	1
11-20	0
21-30	3
31-40	6
Respiratory Insufficiency (No. of patients)	
8	1
9	2
10	1
12	6
Forced Vital Capacity (No. of patients)	
≥80%	3
<80%	4
Not available	3
***Abbreviations: ALS* patients, Amyotrophic Lateral Sclerosis patients; ALS-FRS, Amyotrophic Lateral Sclerosis Functional Rating Scale; s.d., standard deviation**	

As for stroke patients, we also assessed the erythrocyte deformability of ALS patients and compared with control group. The results are presented in Figure IV.9. It could be observed that at low shear stress, that represent larger-diameter vessels, the erythrocytes from ALS patients are more deformable than erythrocytes from control (*** p=0.0004 at 0.3 Pa, *** p<0.0001 at 0.6–3.0 Pa, ** p=0.0041 at 6.0 Pa). High values of shear stress, in smaller diameter vessels, promote an increase of erythrocyte deformability. In smaller diameter vessels, the erythrocytes from ALS patients have a tendency to be more deformable than erythrocytes from control, but the results were not statistically significant.

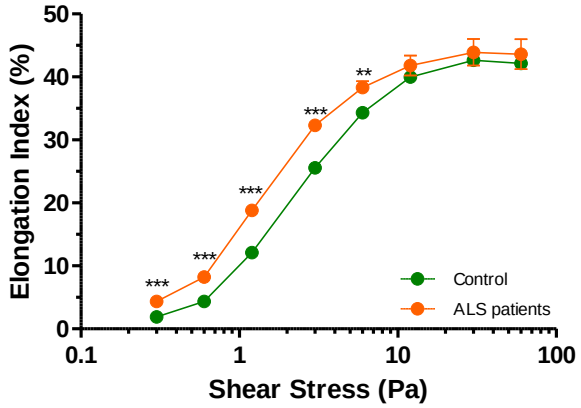

Figure IV.9 - Erythrocyte deformability measured at different shear stress values**.** Variations on erythrocyte deformability by elongation index between ALS patients (n=7) and control group (n=57). Values are presented as mean ±SEM. Statistical significance: *** p=0.0004 at 0.3 Pa, *** p<0.0001 at 0.6–3.0 Pa, ** p=0.0041 at 6.0 Pa.

Other haemorheological parameter that was assessed was the erythrocyte aggregation. In Figure IV.10, the erythrocyte aggregation was measured by the infrared light transmission through a whole blood suspension, at stasis during 5 seconds (*vd.* Figure IV.10a) and 10 seconds (*vd.* Figure IV.10b), with the addition of different fibrinogen concentrations (0.0, 40.0 and 80.0 mg/dL). It could be observed that without addition of fibrinogen, at 5 and 10 seconds, the erythrocytes from ALS patients have a lower tendency to aggregate than the control. With the addition of fibrinogen there was an increase of the erythrocyte aggregation in both groups but the differences between ALS patients and control values were not statistically significant.

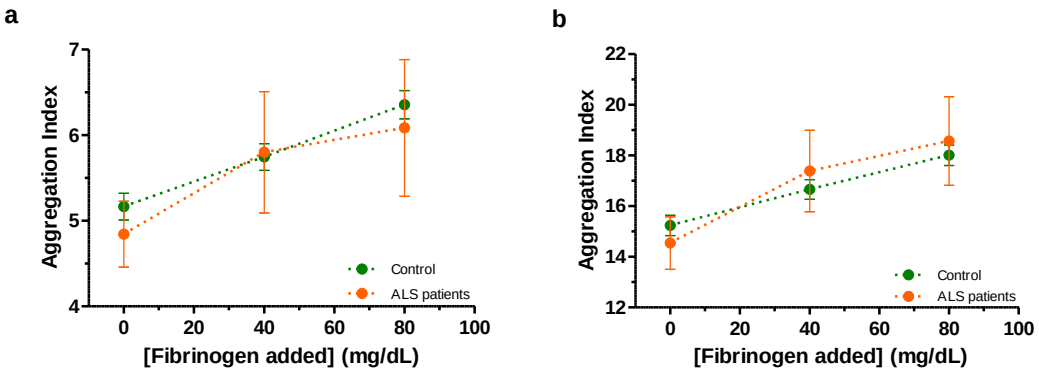

Figure IV.10 - Erythrocyte aggregation measured in function of the fibrinogen addition to blood samples from ALS patients (n=7) and control (n=57), during 5 seconds **(a)** and 10 seconds **(b)**, Values are represented as mean±SEM. This parameter was not statistically significant between the studied groups.

Figure IV.11 shows the results for the whole blood viscosity measured in samples from ALS patients and control at low (22.5 s^{-1}) and high (225 s^{-1}) shear rates, both at a native (*vd.* Figure IV.11a, b, c) and corrected samples with haematocrit of 45% (*vd.* Figure IV.11d, e, f), at 37ºC. The applied shear rate and the diameter of the vessels are inversely proportional mimicking the physiological process. An increase of the shear rate, promotes a decrease of the viscosity of the blood being this related with smaller-diameter vessels (*vd.* Figure IV.11c, f). On the other hand, at low shear rate, there was an

increase of the viscosity, and this occurs in higher diameter vessels (*vd.* Figure IV.11c, f). At native blood viscosity, and low shear rate, the ALS patients are more viscous than the control (p<0.0001). At low shear rate the control has 7.27±0.18 mPa.s *vs.* 9.51±0.90 mPa.s from ALS patients, and for blood viscosity with haematocrit at 45% the control group has 7.22±0.09 mPa.s *vs.* 7.49±0.28 from ALS patients, (*vd.* Figure IV.11a, d, respectively). At high shear rate (*vd.* Figure IV.11b, e), it is observed that the control for native blood viscosity showed a tendency for lower blood viscosity than the ALS patients (4.40±0.08 mPa.s *vs.* 4.80±0.34 mPa.s, respectively). For haematocrit at 45% at high shear rate the tendency is the same for the control and ALS patients (4.51±0.05 mPa.s *vs.* 4.60±0.19 mPa.s, respectively). Both differences were not statistically significant.

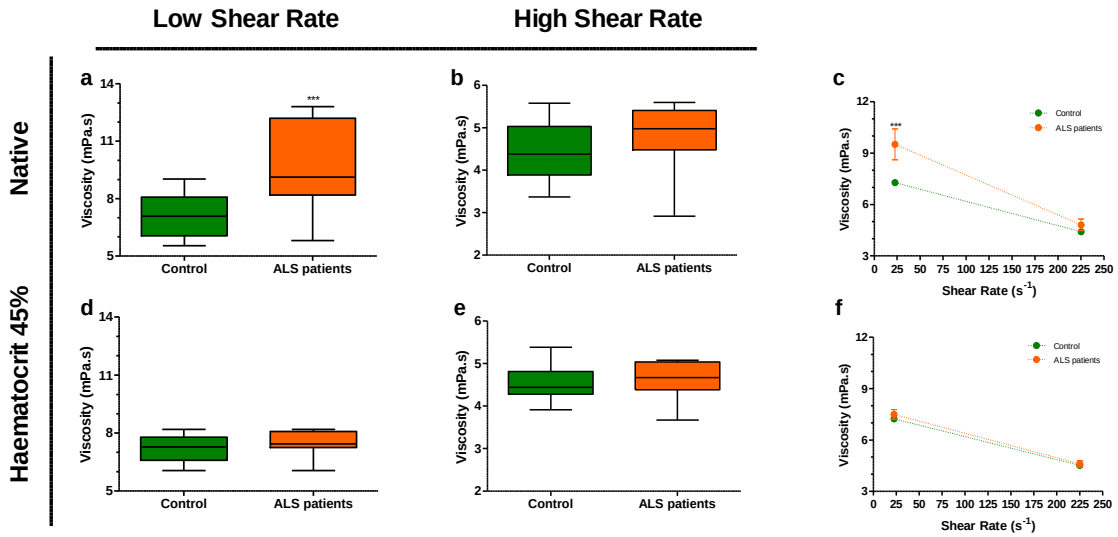

Figure IV.11 - Changes on whole blood viscosity of ALS patients and control. The whole blood viscosity was measured and submitted between ALS patients (n=7) and control (n=57) at low (22.5 s^{-1}) and high (225s^{-1}) shear rates, both at a native **(a, b, c)** and corrected samples with haematocrit of 45% **(d, e, f)**, at 37ºC. Values are presented as box with the median value and whiskers with maximum and minimum values (a,b,d,e) and mean±SEM (c,f). At low shear rate **(a)**, the statistical value is *** p<0.0001. The native blood viscosity at high shear rate did not statistically differ neither the values of blood viscosity with haematocrit at 45% at low and high shear rate (**d, e, f**).

The γ' fibrinogen plasma levels of the ALS patients and control were also quantified (*vd.* Figure IV.12). The increase of γ' fibrinogen plasma levels can results in changes in blood rheological properties. This variant has been associated as a cardiovascular risk factor. Values that fall above the cut-off value (>30 mg/dL, represented by grey dashed line), may be indicative of increased risk of cardiovascular disease. Thus, it could be seen that the ALS patients has higher concentration of γ' fibrinogen in plasma than control (52.55±4.00 mg/dL *vs.* 33.78±1.60 mg/dL, *** p<0.0001, respectively).

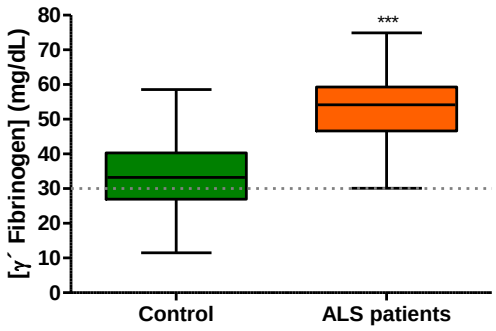

Figure IV.12 - γ' fibrinogen plasma quantification in ALS patients (n=10) and control (n=47). Values are presented as box with median value and whiskers with maximum and minimum values. Cut-off value (>30 mg/dL, represented by grey dashed line), may be indicative of increased risk of cardiovascular disease (*** p<0.0001).

The membrane fluidity of the erythrocytes from control and ALS patients was determined by generalized polarization used laurdan fluorescent probe (*vd.* Figure IV.13). It is known that, in membrane fluidity studies, based on fluorescent generalized polarization of laurdan, the GP values can range from 1 to -1. Negative values are obtained as a consequence of the solvent relaxation phenomenon associated with laurdan-water interactions when membrane lipids are disordered. GP values of erythrocyte from ALS patients were more negative than the ones for control (* p=0.0236). These results indicate that the erythrocyte membrane from ALS patients could be disordered and less compacted than control. Erythrocytes with less compaction of the membrane, when interacts with laurdan can incorporate water molecules into its membrane leading to low GP values. These results could be associated with the possibility of the membrane of the erythrocytes from ALS patients having some alterations in their lipid bilayer composition. The erythrocytes from ALS patients are more fluid than the control.

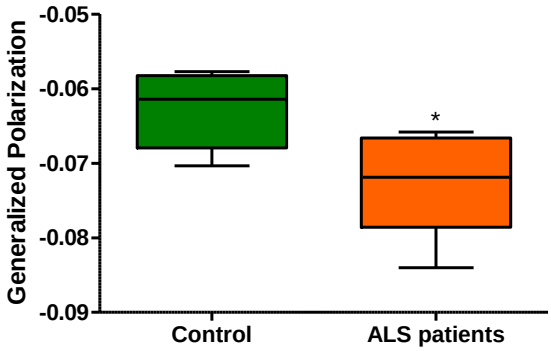

Figure IV.13 - Erythrocyte membrane fluidity measured by fluorescent generalized polarization with laurdan, a fluorescence probe. It was measured erythrocytes from ALS patients (n=7) and control (n=5). Values are presented as box with median value and whiskers with maximum and minimum values (* p=0.0236).

In parallel with the others applied techniques, erythrocyte elasticity measurements in the ALS patients and control group, were also performed (*vd.* Figure IV.14). All the force spectroscopy data were analysed in order to determine the Young's modulus (*vd.* Figure IV.14a) and the penetration depth (*vd.* Figure IV.14b) for each force-distance curve. Erythrocytes from ALS patients are stiffer than the

erythrocytes from control (5032±4792 Pa *vs*. 128.3±19.28 Pa, respectively). The penetration depth (*vd.* Figure IV.14b) was analysed by the position of the maximal movement of the piezo sensor in the z-axis, which corresponds to the z-axis coordinate when the sensor reaches an indentation force of 300 pN, subtracting the z-axis position of the sensor when the tip begins the contact with the surface of the erythrocyte. The erythrocytes from ALS patients have more penetration depth than the erythrocytes from control, indicating that the erythrocytes from ALS patients are more capable to deform than the control (829.6±5.36 nm *vs*. 811.3±7.305 nm, * p=0.0437, respectively).

The elastic properties of the erythrocytes have never been investigated in ALS disease. Changes in viscoelastic properties of the erythrocytes in these patients would have impact on peripheral hypoxia, which is related to tolerance to exercise and functional outcome.

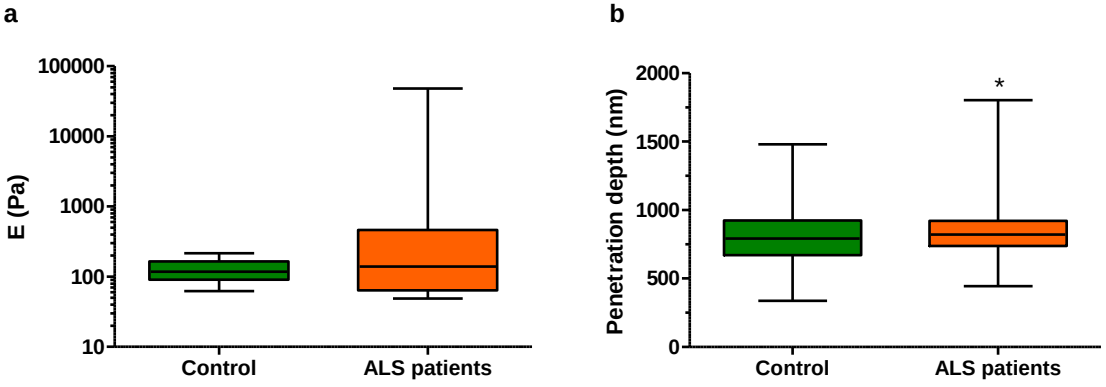

Figure IV.14 - AFM stiffness studies**.** Values of Young's modulus from ALS patients (n=10) and control (n=7). The results are presented as maximum Gaussian peaks (mean±SEM) **(a)**. Penetration depth of the AFM tip on erythrocytes**.** The penetration depth was analysed in erythrocytes from ALS patients (n=10) and control (n=7) by the position of the maximal movement with an indentation force of 300 pN (* p=0.0437) **(b)**. Values are presented as box with median value and whiskers with maximum and minimum values

Performing AFM scanning images of the erythrocytes from ALS patients it was possible to assess their morphology and compare it with the control (*vd.* Figure IV.15). Examples of AFM height and error images obtained for the erythrocytes from ALS patients and controls could be visualized in Table IV.2 of this thesis. Results of the erythrocytes diameter could be analysed on Figure IV.15a. It can be observed that the erythrocytes from ALS patients have higher diameter than erythrocytes from control (8.513±0.018 µm *vs*. 8.296±0.016 µm, *** p<0.0001, respectively). The area of the erythrocytes from ALS patients was also higher than the control (57.23±0.23 μm^2 *vs*. 54.19±0.16 μm^2, *** p<0.0001, respectively) (*vd.* Figure IV.15b). Erythrocytes from ALS patients were also taller than erythrocytes from control (0.593±0.002 µm *vs*. 0.572±0.003 µm, *** p<0.0001, respectively) (*vd.* Figure IV.15c). Erythrocyte from ALS patients have slightly less volume than erythrocytes from control (21.10±0.25 μm^3 *vs*. 21.81±0.22 μm^3,* p=0.0315, respectively) (*vd.* Figure IV.15d). Erythrocytes from ALS patients had a larger distribution of the morphological values than the control.

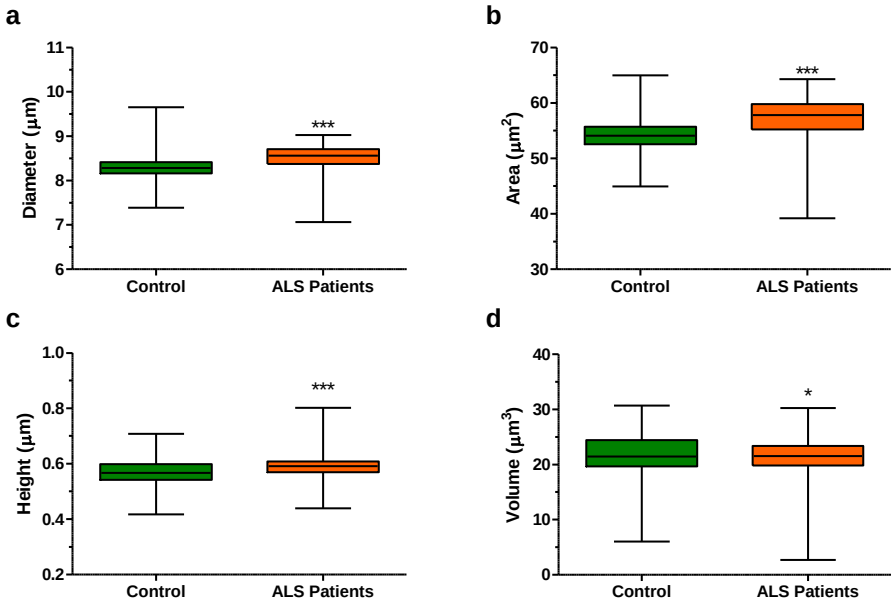

Figure IV.15 - Results of AFM scanning imaging of erythrocytes from ALS patients (n=10) and control (n=7). Morphological characterization of erythrocytes, throught the analysis of different parameters: diameter **(a)**, area **(b)**, height **(c)** and volume **(d)**.Values are presented as box with median value and whiskers with maximum and minimum values. Statistical values represents are: **(a, b, c)** *** $p<0.0001$, **(d)** * $p=0.0315$.

Another parameter that could be assessed through the analysis of the AFM images of the erythrocytes was the surface roughness (*vd.* Figure IV.16). Erythrocyte membrane roughness average (Ra) was assessed (*vd.* Figure IV.16a) which is defined by the mean of the absolute values of the height of the surface profile. From the results it could be observed that the average roughness (Ra) of the erythrocytes from ALS patients is lower than the control. Thus, the surface of the erythrocyte from ALS patients was less rough than the surface of the erythrocytes from control (1.31±0.07 nm *vs*. 1.72±0.15 nm, * $p=0.0176$, respectively). Values of the Root Mean Square Roughness (Rq) were also analysed (*vd.* Figure IV.16b). This parameter is more specific for the measurement of the surface roughness because it can distinct the peaks and valleys on the surface profile. Thus, the surface of the erythrocytes from ALS patients have less membrane profile perturbances which means that is less rough than the surface of the erythrocytes from the control (1.73±0.08 nm *vs*. 2.13±0.19 nm, * $p=0.0479$, respectively).

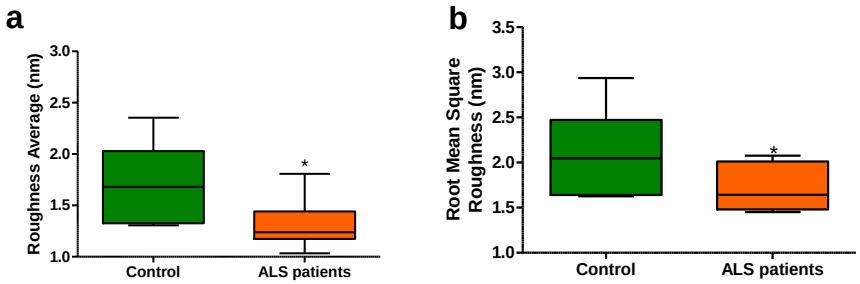

Figure IV.16 – Erythrocyte membrane roughness of control (n=7) and ALS patients (n=10). The average roughness (Ra) **(a)** and Root Mean Square Roughness (Rq) **(b)** were measured. Values are presented as box with median value and whiskers with maximum and minimum values. Statistic values represented are: **(a)** * $p=0.0176$, **(b)** * $p=0.0479$.

Zeta-Potential of the erythrocytes was also assessed (*vd.* Figure IV.17) to analyse the variation of the electrostatic forces in erythrocytes from ALS patients and control, in the absence or in the presence of different fibrinogen concentrations. Without the addition of fibrinogen it could be observed that the erythrocytes from ALS patients have a more positive surface charge than the control, (-12.18±0.06 mV *vs*. -12.80±0.09 mV, *** p<0.0001, respectively) (*vd.* Figure IV.17a). When fibrinogen (0.4 mg/mL) was added, the charge of the erythrocytes from ALS patients altered and stays more positive than control (-10.85±0.08 mV *vs*. -11.23±0.11 mV, ** p=0.0087, respectively). Increasing the addition of fibrinogen the charge of the erythrocytes became even more positive in both samples, but without statistically significant differences between them (*vd.* Figure IV.17b). At higher concentration of fibrinogen, the membranes of the erythrocytes could be saturated of fibrinogen molecules leading only to a slightly variation of the charge of the cellular membrane. The Δζ curves (*vd.* Figure IV.17c) have a tendency to achieve a plateau at high concentration of fibrinogen (~ 2 mg/mL). From these curves it could hypothesized that the erythrocyte membranes of ALS patients became saturated with less number of fibrinogen molecules added. This fact could be explained by the less negatively charged membranes of the erythrocyte from ALS patients when no fibrinogen molecules were added.

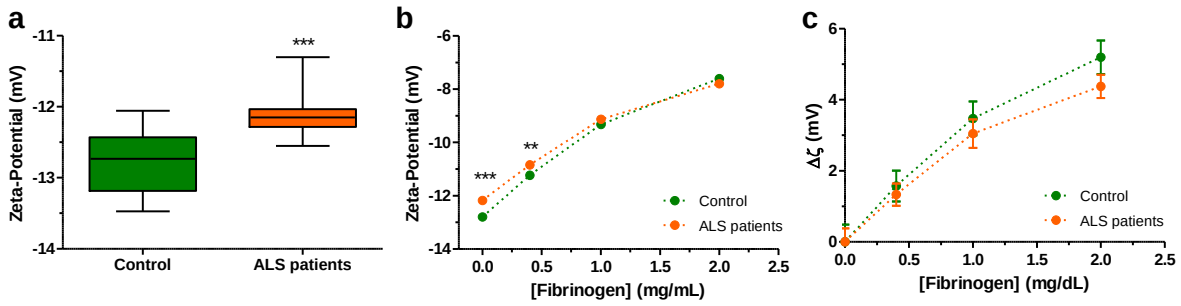

Figure IV.17 - Zeta-potential of the erythrocytes from ALS patients (n=10) and control (n=7), without **(a)** and with addition of different concentrations of fibrinogen **(b)**. Values are presented as box with median value and whiskers with maximum and minimum values **(a)**. The values are presented as mean ±SEM **(b)**. Variation of zeta-potential of the erythrocytes **(c)**. Statistic values represented are: **(a)** *** p<0.0001; **(b)** *** p<0.0001 and ** p=0.0087.

Other zeta-potential studies were performed with erythrocytes from healthy donors and in the presence of different concentrations of fibrinogen variants (γAγA and γAγ' fibrinogen). In Figure IV.18a it could be observed that, without the presence of fibrinogen, the erythrocyte membrane has a value of zeta-potential of -12.80±1.10 mV, which is lower than in the presence of fibrinogen concentration. At 0.4 mg/mL of γAγA and γAγ' fibrinogen, there was no significant variation of zeta-potential between both variants (-11.92±0.60 mV *vs.* -11.96±0.93 mV, respectively). The negatively charge erythrocyte membrane has high affinity for fibrinogen molecules. Thus its membrane charge became more positive due to the binding of fibrinogen on the erythrocyte membrane. At 0.7 mg/mL of fibrinogen concentration, the membrane charge of erythrocyte in the presence of the γAγ' fibrinogen is more positive than in the presence of γAγA fibrinogen (-11.88±0.65 mV *vs.* -12.22±0.78 mV, respectively). It could be hypothesized that γAγ' fibrinogen has higher affinity for erythrocyte membrane than γAγA fibrinogen. Figure IV.18b shows the values of the variation of Zeta-Potential (Δζ) for each sample

which was calculated by subtracting the zeta-potential value of the erythrocytes in the presence of fibrinogen by the initial value (corresponding to the value of Δζ at zero fibrinogen concentration). From the results it could be seen that γAγA fibrinogen at 0.4 mg/mL has higher affinity for erythrocyte membrane than γAγ' fibrinogen. Also, at 0.7mg/mL of γAγA fibrinogen the value of Δζ did not vary significantly and the curve achieve a plateau. This could mean that, at γAγA fibrinogen concentration higher than 0.4 mg/mL, the erythrocyte membrane is saturated with fibrinogen molecules attached to it. At all γAγ' fibrinogen concentrations tested on this study, the erythrocytes membrane did not reach the saturation (*vd.* Figure IV.18b).

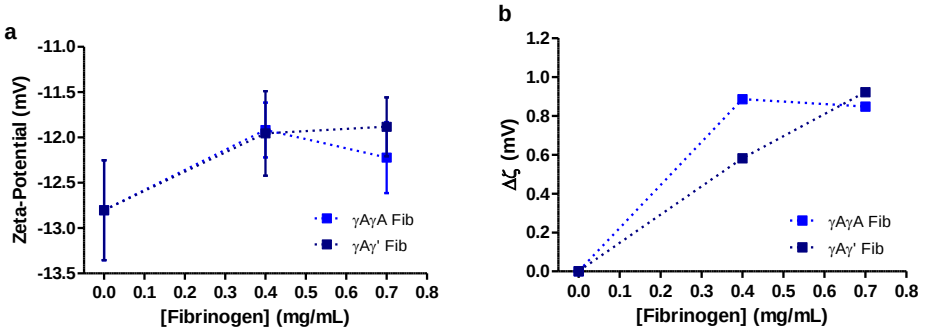

Figure IV.18 - Zeta-potential of erythrocytes from healthy donors (n=4) in the absence and in presence of different concentrations (0.4 and 0.7 mg/ml) of the fibrinogen (γAγA and γAγ' variants) **(a)**. Variation of the zeta-potential (Δζ) for the same erythrocytes and conditions **(b)**. Values are represented as mean ± SEM.

It is known that a deviation of the zeta-potential to more positive values can be associated with the removal of sialic acid, because it is the principal source of the negative charge on the erythrocytes membrane (Carvalho *et al.*, 2011; Fernandes *et al.*, 2011). Therefore in control conditions, the presence of γAγ' fibrinogen promotes less reduction of sialic acids on erythrocyte membrane and has less interaction with it. This study is important for comprehension the changes of the charge of the erythrocyte membrane, and their relation with affinity, interaction and adhesion to γAγ' fibrinogen, that is related with high cardiovascular risk events. This part of the study was only performed with erythrocytes from healthy donors due to the low amount of fibrinogen solution available in the laboratory for conducting these experiments (especially γAγ' fibrinogen). Knowing that ALS patients has higher fibrinogen γAγ' concentration in the plasma than healthy donors (*vd.* Figure IV.12), in the future, it will be extremely important to conduct the same experiments but with erythrocytes isolated from ALS patients.

2.1) Special clinical cases

Knowing all the results from ALS patients it is possible to highlight three clinical cases.

ALS patient I, represented by the purple colour point in the graphics, is a 43-years-old woman with diagnostic of amyotrophic lateral sclerosis with a spinal onset form, a score of 27 in ALS-FRS scale, and a total survival time of 1.3 years before the date of blood collection for this study. This patient had a deep venous thrombosis event on the day before the collection of the blood. **ALS patient II,**

represented by the blue point in the graphics, is a 72-years-old man with diagnostic of ALS spinal onset form, a score of 10 in ALS-FRS scale, and a total survival time of 21.7 years before the date of blood collection. **ALS patient III,** represented by the grey point in the graphics, is a 73-years-old man with diagnostic of ALS and a total survive time of 2.5 years before the date of blood collection. This patient has the respiratory onset form and a score of 29 in ALS-FRS scale. The graphics below (*vd.* Figure IV.19 to Figure IV.25) are identical to the ones already shown above, but highlighting the specific colours of each special clinical case.

On Figure IV.19, it could be observed that ALS patient II have the lowest viscosity of all ALS patients studied, at low and high shear rate and in native whole blood or with haematocrit correction at 45%. This haemorheological parameter has not been measured for ALS patient I. The ALS patient III has a value of viscosity close to the mean for the whole blood viscosity.

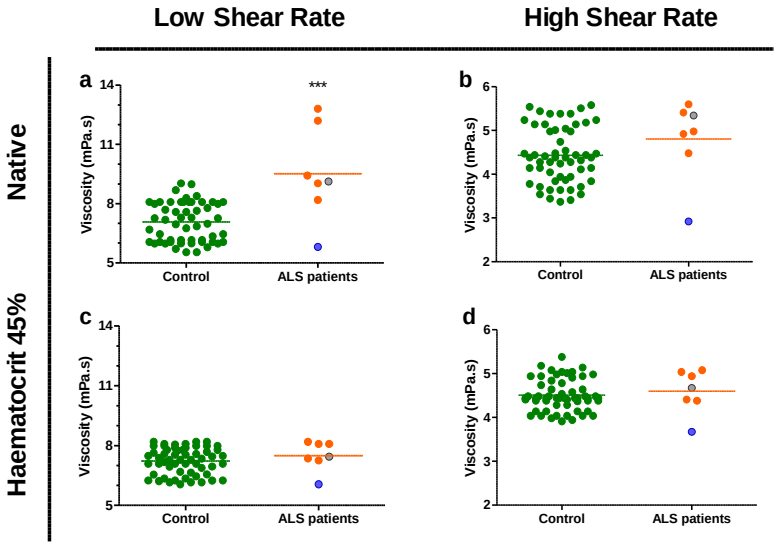

Figure IV.19 - Variations on whole blood viscosity of ALS patients (n=7) and control (n=57) at low (22.5 s^{-1}) and high (225s^{-1}) shear rates, both at a native **(a, b)** and corrected samples with haematocrit of 45% **(d, e)**, at 37ºC. ALS patient II (blue point) and ALS patient III (grey point) are highlighted.

All ALS patients have γ' fibrinogen concentration values above the cut-off value (>30mg/dL) (*vd.* Figure IV.20). ALS patient I has one of the lowest value of the γ' fibrinogen in plasma, but ALS patients II and III presented high levels of γ' fibrinogen in plasma. These patients are much older than the ALS patient I. Thus, this result can indicate that the increase of the γ' fibrinogen quantification in plasma could be associated with increasing the age of patient, and also with increasing risk of cardiovascular disease. This result is contradictory with the fact that ALS patient I is the one that had a deep venous thrombosis event. It is not reported any cardiovascular disease event in patients ALS II and III clinical history.

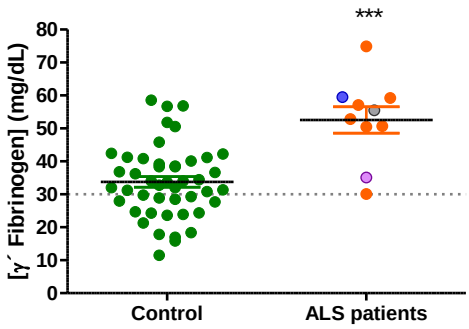

Figure IV.20 - γ' Fibrinogen plasma quantification in ALS patients (n=10) and control (n=47) by semi-automated quantitative ELISA method. Values that fall above the cut-off value (>30 mg/dL, represented by grey dashed line), may be indicative of increased risk of cardiovascular disease (*** p<0.0001). ALS I patient (purple point), ALS patient II (blue point) and ALS patient III (grey point) are highlighted.

Erythrocyte membrane fluidity was only possible to be determined on ALS patients II and III. ALS patient II has the more negative value of GP than all the ALS patients. By the contrary, the erythrocyte fluidity of ALS patient III was the less negative. This could mean that the erythrocyte membranes of ALS patient III could be more ordered and high compacted. One of the main clinical differences between patients II and III is that patient II has a spinal onset form and patient III has a respiratory onset form. Whether this could explain or not these differences in erythrocyte membrane fluidity is a subject that will need to be clarified. These results indicate that the erythrocyte membrane from ALS patients can be disordered and less compacted than control.

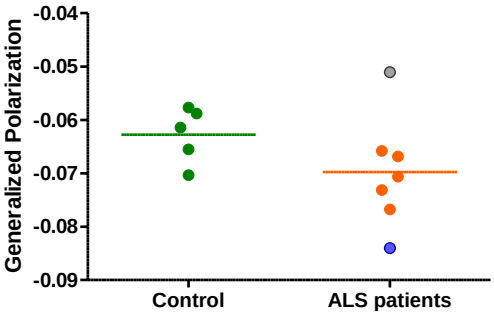

Figure IV.21 - Erythrocyte membrane fluidity study based with fluorescent generalized polarization of laurdan, a fluorescence probe. ALS patient II (blue point) and ALS patient III (grey point) are highlighted

From the erythrocyte membrane zeta-potential data it was possible to observe that ALS patient III has more positively charge of the membrane of the erythrocyte than the others patients. ALS patient I and II had values approximately the same as the mean of the ALS patients group. The fact that the erythrocyte membrane from ALS patient III is more positively charge and less fluid could be associated with their respiratory failure.

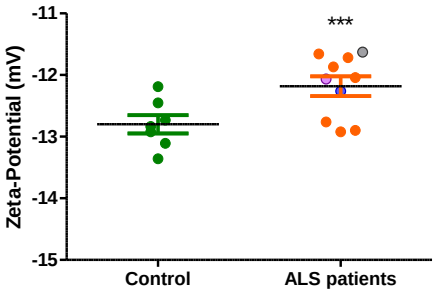

Figure IV.22 - Zeta-potential of erythrocytes from ALS patients (n=10) and control (n=7), without fibrinogen addition (*** p<0.0001). ALS I patient (purple point), ALS patient II (blue point) and ALS patient III (grey point) are highlighted.

The Young's modulus of the erythrocytes and the penetration depth of the same ALS patients were analysed. ALS patient I, represented at purple point, has the highest value of the Young's modulus and the lowest value of the erythrocyte penetration depth (*vd.* Figure IV.23). ALS patient II (blue point) had also a high value of the Young's modulus. ALS patient III, the grey point, had a medium value of the Young's modulus but a low value of the erythrocyte penetration depth. ALS patient I had stiffer erythrocytes and less deformable which could be associated with a higher risk of having a cardiovascular event. In fact a deep venous thrombosis event was reported on the clinical history of this patient on the day before the collection of the blood.

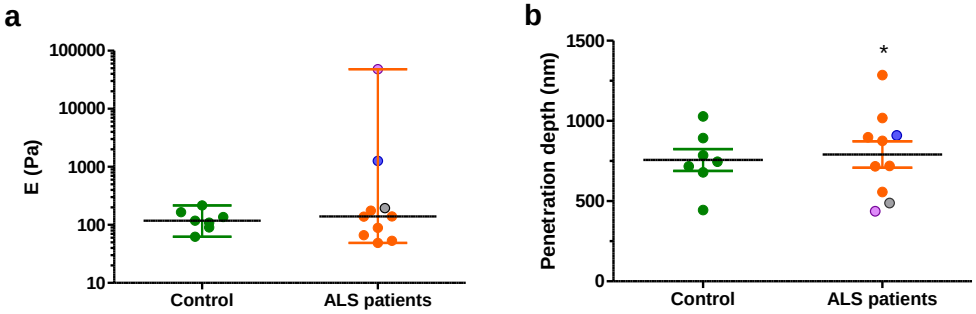

Figure IV.23 – Erythrocyte stiffness by Atomic Force Microscopy in ALS patients *vs* control. Young's modulus **(a)** and penetration depth of the AFM tip on erythrocytes **(b)**. ALS I patient (purple point), ALS patient II (blue point) and ALS patient III (grey point) are highlighted.

In Table IV.2, it could be observed some examples of AFM height and error images obtained for the control and for ALS patients (I, II and III).

Table IV. 2 - Morphological properties of erythrocytes measured by atomic force microscopy from control and ALS patients (ALS patient I, II and III). Column A: AFM height image with relative colour scale (80 µm × 80µm). Column B: the respective AFM error signal image. Column C: examples of the morphological analysis of the erythrocytes done using a specific software (SPIP™ software, Image Metrology, Inc.).

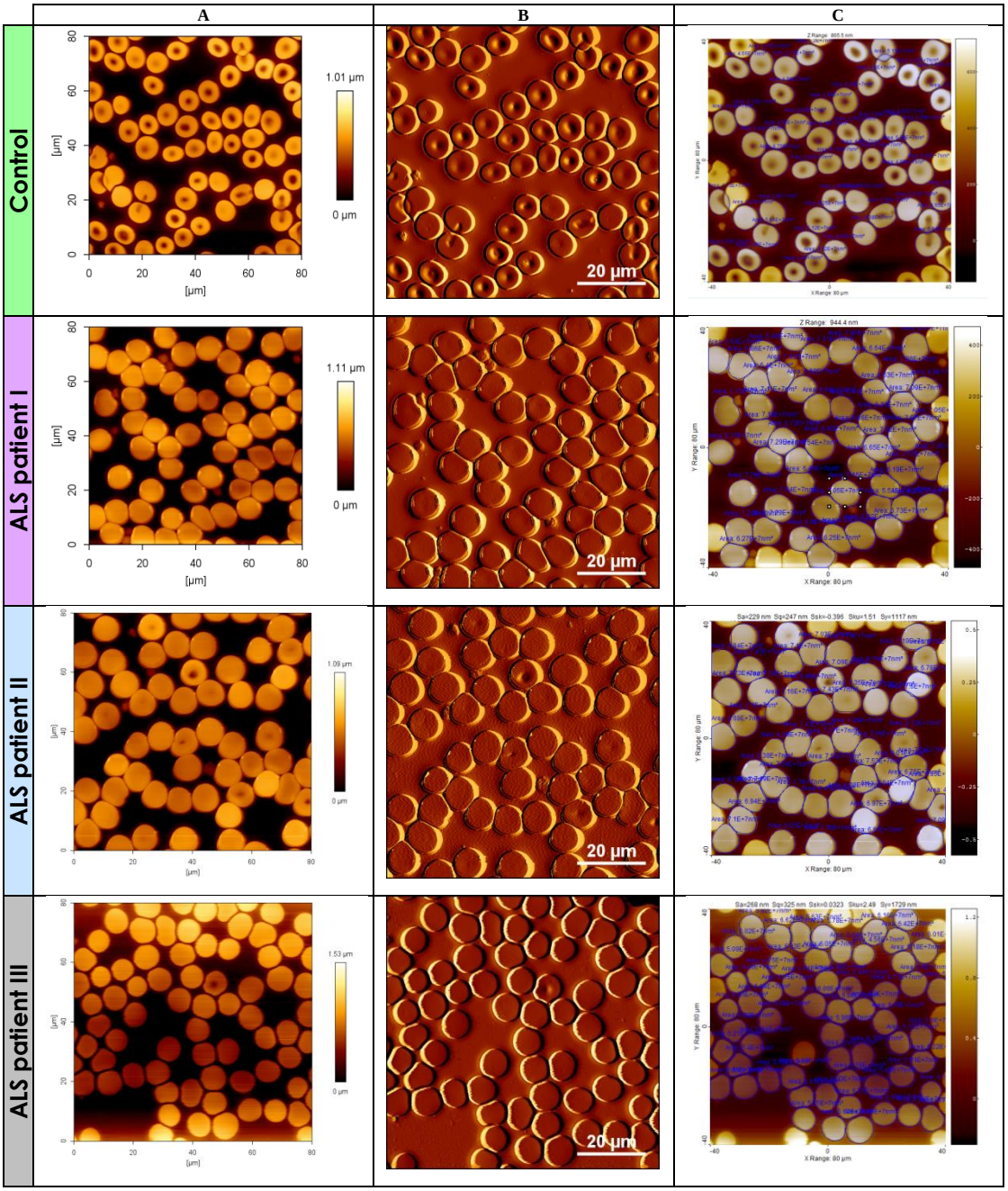

Analysing Table IV.2, it could be observed that exists differences between the erythrocytes from control and ALS patients.

In Figure IV.24, it could be observed that ALS patient I had values for the erythrocytes morphology close to the average value of the ALS patient group. On ALS patient II, the erythrocytes have higher diameter and area, but have lower volume than the average value of all the ALS patients. The

erythrocytes from ALS patient III were taller and had more volume than erythrocytes from others ALS patients.

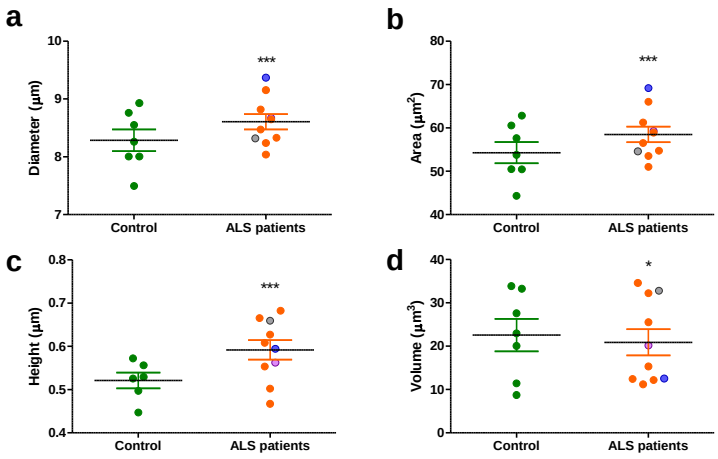

Figure IV.24 - Morphological characterization of erythrocytes by the analysis of AFM scanning images from ALS patients and control. The erythrocyte diameter **(a)**, area **(b)**, height **(c)** and volume **(d)** were measured. ALS I patient (purple point), ALS patient II (blue point) and ALS patient III (grey point) are highlighted.

ALS patient I and II have higher erythrocyte surface roughness (Root Mean Square Roughness) than the erythrocytes from all ALS patients (*vd.* Figure IV.25).

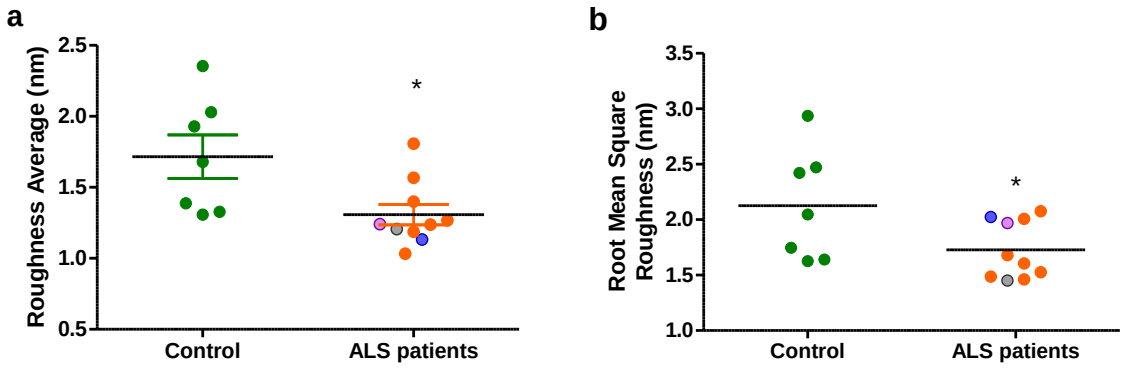

Figure IV.25 - Erythrocyte membrane roughness of control and ALS patients. The average roughness (Ra) **(a)** and Root Mean Square Roughness (Rq) **(b)** were measured. ALS I patient (purple point), ALS patient II (blue point) and ALS patient III (grey point) are highlighted.

It has been associated with Amyotrophic Lateral Sclerosis an elevated risk for venous thromboembolism. On this study it was investigated the importance of different parameters to understand which morphological changes and interactions of the erythrocytes exists on ALS patients.

From the AFM results, it was possible to assess the erythrocyte morphological and elastic properties and conclude that erythrocytes from ALS patients are higher and taller, and have less membrane roughness than the controls. They also have more penetration depth and a tendency to be stiffer than the erythrocytes from control. These results indicate that, in ALS disease, it occurs changes on erythrocyte membrane. D' Angelo *et al*. (2013) shown that the proteins and peptides are susceptible to a variety of chemical modifications that can affect their structure and biological functions (D'Angelo

et al., 2013). The composition of the membrane of the erythrocyte could be changed, and among these modifications, the isomerization of aspartic acid and deamination of asparagine occur in proteins and peptides during cell aging. Cytoplasmatic enzymes can also decline during erythrocyte aging (Carvalho *et al.*, 2011). The enhanced deamidation/isomeration of the erythrocyte membrane proteins may affect the phenotype of the pathophysiology of the disease (D'Angelo *et al.*, 2013). A variety of induced stress conditions, including oxidation, has been shown to significantly increase the isoaspartate residue content in erythrocytes. It has been demonstrated that specific erythrocyte membrane proteins, among which, in particular, cytoskeletal components are substrates for the methyltransferase (D'Angelo *et al.*, 2013). The young's modulus and penetration depth are higher. This could be due to changes in the cytoskeletal components, such as the bands 2.1 (ankyrin) and 4.1, which are the proteins that provide some rigidity to the membrane (D'Angelo *et al.*, 2013). Other changes on erythrocyte membrane components and organization are associated with the age of the erythrocytes, which include changes on carbohydrates (exposure of b-galactosyl residues that are recognized by lectin-like receptors), proteins (e.g., modification of band 3 protein) and decrease on the activities of several enzymes (including enzymes of the glycolytic and pentose shunt pathways, involved in cell thiol metabolism and protection against oxidative damage) (Carvalho *et al.*, 2011). Other important component of the membrane in erythrocytes is the glycophorin A, a major sialoglycoprotein of human erythrocyte membrane. It is the major contact or receptor membrane polypeptide that also spans the lipid bilayer. This network is tethered to the cell membrane mediated by ankyrin that couples spectrin to band 3 and the other mediated by protein 4.1 that couples the junctional complex to glycophorin C/D (Kim *et al.*, 2015). Knowing the results of membrane fluidity, lower generalized polarization of the erythrocytes from ALS patients could be associated with the lipid composition of the membrane and lipid packing. The band 3 is an anion channel, which is responsible for water and anion transportation. It is a major transmembrane glycoprotein in erythrocyte, and it transport anions by proteolytic cleavage or aggregation. Negative values of the membrane fluidity are associated with water penetration in the membrane when the probe gets in phospholipid bilayer. Thus, these changes on erythrocyte membrane in ALS allow the internalization of water molecules and promoted lower packing and membrane fluidity. Zeta-potential results showed that the erythrocytes from ALS patients have less electronegativity on its surface. These results can be explained by the possible differences on the number of sialic acids that constitute the erythrocyte membrane. The sialic acid content of cellular membranes may account for up to half of the negative charge of the cell surface (Nanetti *et al.*, 2008). The negatively charged of the sialic acids stabilize glycoprotein conformation in cell surface receptors to increase cell rigidity. The rigidity of the erythrocytes from ALS patients was also altered. This can be due to the glycophorin A that could also be modified. In our previous studies (Carvalho *et al.*, 2011), we observed that the removal of the number of sialic acids decreases the percentage of fibrinogen-erythrocyte receptor binding events, without significantly affecting the (un)binding forces of each interaction. An alteration in the lipid composition

(phospholipids, glycolipids) and loss of asymmetry between the inner and outer leaflets of the lipid bilayer is also associated with erythrocytes senescence. The interaction between phosphatidylserine and the cytoskeleton component spectrin triggers the accumulation of large amounts of phosphatidylserine and phosphatidylethanol amine on the outer leaflet erythrocyte membrane (Carvalho *et al.*, 2011). Thus, a possible reduction of the sialic acid content in membrane of the erythrocytes from ALS patients could promote a more positive membrane charge, as shown by our results.

In parallel with these results, it was possible to conclude that erythrocytes from ALS patients are more deformable with increasing the shear stress values. These results confirm the AFM stiffness results, because the erythrocytes from ALS patients are stiffer and have more penetration depth than control. About the erythrocyte aggregation (with the addition of the fibrinogen) the erythrocytes from ALS patients have more tendency to increase its aggregation. So a decrease of membrane sialic acids content may contribute to the erythrocytes transient aggregation in circulation. The blood from ALS patients are more viscous and have more γ' fibrinogen content in plasma. This parameter has been associated with an elevated cardiovascular risk factor, and venous thrombotic risk. When the fibrin clots are formed in the presence of the γ' fibrinogen, they are more resistant to fibrinolysis. Furthermore, the γ' chain contains a binding site for thrombin, and clots made from γ' fibrinogen have been reported to have altered clot architecture (Domingues *et al.*, 2016). So, ALS patients have higher risk of venous thrombosis, due to the elevated γ' fibrinogen concentration in their plasma. An increase in erythrocyte membrane aggregation has also been considered as a cardiovascular risk factor. Therefore changes on these erythrocyte parameters could promote thrombolytic events, in ALS patients.

V) General Conclusions and Future Work

The purposes of this project were (i) to study the influence of fibrinogen on erythrocytes adhesion in stroke patients; and (ii) to evaluate morphological and elasticity changes on erythrocytes from ALS patients. Erythrocytes from stroke patients were evaluated by their haemorheological properties and by atomic force microscopy. Atomic force microscopy was used to measure fibrinogen-erythrocyte interaction, erythrocytes stiffness and erythrocyte-erythrocyte adhesion, in the presence of different fibrinogen concentrations. Atomic force microscopy-based force spectroscopy measurements, at the single-molecule level, showed that the fibrinogen-erythrocyte binding forces are increased in stroke patients, despite its lower binding frequency. Erythrocyte-erythrocyte adhesion showed that, with increasing fibrinogen concentrations, the work and the maximum force necessary to detach two erythrocytes are increased. Thus, erythrocytes from stroke patients have more tendency to aggregate. Additionally, these patients have an increase of the plasma γ' fibrinogen concentrations and have more viscous blood. Stiffness studies revealed that erythrocytes from stroke patients are less deformable than the control. All these alterations of the erythrocytes from stroke patients are significant risk factors for a bad prognostic of the stroke disease. Also it has to be taken in consideration that the binding between fibrinogen and erythrocyte could be a new cardiovascular risk factor for stroke disease.

Erythrocytes from ALS patients were also evaluated by their haemorheological behaviour and by atomic force microscopy. AFM was used to measure stiffness and evaluate morphological changes of the erythrocyte from ALS patients. The results revealed that erythrocytes from ALS patients are more capable to deform than the control. Changes on their erythrocyte morphology were also found. Erythrocytes from ALS patients have a less rough membrane than the control and the cells have higher area and height. Moreover, ALS patients have an increase of the plasma γ' fibrinogen concentrations and the blood is more fluid. Furthermore, membrane fluidity and zeta-potential studies in erythrocytes from ALS patients revealed that the erythrocyte membrane has changed. These changes in erythrocyte membrane could promote interactions between fibrinogen and erythrocytes and between two erythrocytes which as to be considered a risk factor for thromboembolism venous event.

Therefore, using AFM and others biophysical techniques, it was possible to evaluate the physico-chemical-electrical, mechanical and morphological properties of the erythrocytes from patients with stroke or ALS disease. The results could help to understand the role of fibrinogen on erythrocyte aggregation, and others parameters (*eg.* membrane lipid composition), which may be relevant for potential future drug interventions to reduce aggregation and enhance microcirculatory flow conditions in patients with venous thromboembolism risk.

These results were achieved with a smaller group of stroke (n=6) and ALS (n=10) patients. In the future, it is important to enlarge the number of the samples to have a more pronounced effects of both diseases on the studied parameters. Also, our findings could contribute to dissect the complex

interplay between respiratory function, progression rate, lipid profile and survival in ALS. This could help to find a molecular biomarker of early respiratory dysfunction in ALS patients that could comprise prognostic value.

Finally the role of membrane changes of erythrocytes in tissue hypoxia is a relevant novel issue that deserves appropriate investigation. Only increasing the number of the patients and confirming our findings it will be possible to translate them for clinical application.

VI) References

Aleman, M.M., Walton, B.L., Byrnes, J.R. & Wolberg, A.S. (2014) Fibrinogen and red blood cells in venous thrombosis. *Thrombosis research*, **133**, S38-40.

Alkuraishy, H.M., Al-Gareeb, A.I. & Albuhadilly, A.K. (2014) Vinpocetine and Pyritinol: A New Model for Blood Rheological Modulation in Cerebrovascular Disorders-A Randomized Controlled Clinical Study. *BioMed Research International*, **2014**, 1–8.

Ariëns, R.A.S. (2013) Fibrin(ogen) and thrombotic disease. *Journal of thrombosis and haemostasis : JTH*, **11**, 294–305.

Averett, L.E. & Schoenfisch, M.H. (2010) Atomic force microscope studies of fibrinogen adsorption. *The Analyst*, **135**, 1201–9.

Baskurt, O.K. & Meiselman, H.J. (2003) Blood rheology and hemodynamics. *Seminars in thrombosis and hemostasis*, **29**, 435–50.

Baskurt, O.K. & Meiselman, H.J. (2007) Hemodynamic effects of red blood cell aggregation. *Indian Journal of Experimental Biology*, **45**, 25–31.

Bernardes, N., Abreu, S., Carvalho, F.A., Fernandes, F., Santos, N.C. & Fialho, A.M. (2016) Modulation of membrane properties of lung cancer cells by azurin enhances the sensitivity to EGFR-targeted therapy and decreased β1 integrin-mediated adhesion. *Cell cycle (Georgetown, Tex.)*, **15**, 1415–24.

Berry, J.D. & Korngut, L. (2014) Reevaluating the risk of DVT in people with ALS: weak in the knees and DVTs. *Neurology*, **82**, 1668–9.

Bowman, K., Saffell, J., Cell, D., Biology, M. & London, I.C. (2012) Measuring the cell-cell adhesion force exerted by a cell adhesion molecule. *JPK Instruments AG*, 1–4.

Brown, A.E.X., Litvinov, R.I., Discher, D.E., Purohit, P.K. & Weisel, J.W. (2009) Multiscale Mechanics of Fibrin Polymer: Gel Stretching with Protein Unfolding and Loss of Water. *Science*, **325**, 741–744.

Cannon, B. (2013) Cardiovascular disease: Biochemistry to behaviour. *Nature*, **493**, S2-3.

Carvalho, F.A., Connell, S., Miltenberger-Miltenyi, G., Pereira, S.V., Tavares, A., Ariëns, R. a S., *et al.* (2010) Atomic force microscopy-based molecular recognition of a fibrinogen receptor on human erythrocytes. *ACS Nano*, **4**, 4609–4620.

Carvalho, F.A., Freitas, T. & Santos, N.C. (2015) Taking nanomedicine teaching into practice with atomic force microscopy and force spectroscopy. *Advances in Physiology Education*, **39**, 360–366.

Carvalho, F.A., Martins, I.C. & Santos, N.C. (2013) Atomic force microscopy and force spectroscopy on the assessment of protein folding and functionality. *Archives of Biochemistry and Biophysics*, **531**, 116–127.

Carvalho, F.A., Oliveira, S. de, Freitas, T., Gonçalves, S. & Santos, N.C. (2011) Variations on fibrinogen-erythrocyte interactions during cell aging. *PloS one*, **6**, e18167.

Carvalho, F.A. & Santos, N.C. (2012) Atomic force microscopy-based force spectroscopy - Biological and biomedical applications. *IUBMB Life*, **64**, 465–472.

Cazaux, S., Sadoun, A., Biarnes-Pelicot, M., Martinez, M., Obeid, S., Bongrand, P., *et al.* (2016) Synchronizing atomic force microscopy force mode and fluorescence microscopy in real time for immune cell stimulation and activation studies. *Ultramicroscopy*, **160**, 168–181.

Chida, K., Sakamaki, S. & Takasu, T. (1989) Alteration in autonomic function and cardiovascular regulation in amyotrophic lateral sclerosis. *Journal of neurology*, **236**, 127–30.

Chiò, A., Calvo, A., Bovio, G., Canosa, A., Bertuzzo, D., Galmozzi, F., *et al.* (2014) Amyotrophic lateral sclerosis outcome measures and the role of albumin and creatinine: a population-based study. *JAMA neurology*, **71**, 1134–42.

Cox, T.R. & Erler, J.T. (2011) Remodeling and homeostasis of the extracellular matrix: implications for fibrotic diseases and cancer. *Disease models & mechanisms*, **4**, 165–78.

D'Angelo, S., Trojsi, F., Salvatore, A., Daniele, L., Raimo, M., Galletti, P., *et al.* (2013) Accumulation of altered aspartyl residues in erythrocyte membrane proteins from patients with sporadic amyotrophic lateral sclerosis. *Neurochemistry International*, **63**, 626–634.

De Oliveira, S., Vitorino de Almeida, V., Calado, A., Rosário, H.S. & Saldanha, C. (2012) Integrin-associated protein (CD47) is a putative mediator for soluble fibrinogen interaction with human red blood cells membrane. *Biochimica et biophysica acta*, **1818**, 481–90.

Domenech, O., Dufrêne, Y.F., Bambeke, F. Van, Tukens, P.M. & Mingeot-Leclercq, M.-P. (2010) Interactions of oritavancin, a new semi-synthetic lipoglycopeptide, with lipids extracted from Staphylococcus aureus. *Biochimica et biophysica acta*, **1798**, 1876–85.

Domingues, M.M., Macrae, F.L., Duval, C., McPherson, H.R., Bridge, K.I., Ajjan, R.A., *et al.* (2016) Thrombin and fibrinogen γ' impact clot structure by marked effects on intrafibrillar structure and protofibril packing. *Blood*, **127**, 487–495.

Domingues, M.M., Santiago, P.S., Castanho, M.A.R.B. & Santos, N.C. (2008) What can light scattering spectroscopy do for membrane-active peptide studies? *Journal of Peptide Science*, **14**, 394–400.

Donner, M. & Stoltz, J.F. (1985) Lipid fluidity of red cell membranes assessed with different fluorescent probes. *Acta médica portuguesa*, **6**, S27-30.

Dzierzak, E. & Philipsen, S. (2013) Erythropoiesis: development and differentiation. *Cold Spring Harbor perspectives in medicine*, **3**, 1–16.

Farrell, D.H. (2014) GammaCoeur Semi-Automated ELISA Assay. *Gamma Therapeutics*.

Fernandes, H.P., Cesar, C.L. & Barjas-Castro, M. de L. (2011) Electrical properties of the red blood cell membrane and immunohematological investigation. *Revista brasileira de hematologia e hemoterapia*, **33**, 297–301.

Fotiadis, D. (2012) Atomic force microscopy for the study of membrane proteins. *Current opinion in biotechnology*, **23**, 510–5.

Freire, J.M., Domingues, M.M., Matos, J., Melo, M.N., Veiga, A.S., Santos, N.C., *et al.* (2011) Using zeta-potential measurements to quantify peptide partition to lipid membranes. *European biophysics journal : EBJ*, **40**, 481–7.

Gdynia, H.-J., Kurt, A., Endruhn, S., Ludolph, A.C. & Sperfeld, A.-D. (2006) Cardiomyopathy in motor neuron diseases. *Journal of neurology, neurosurgery, and psychiatry*, **77**, 671–3.

Gladman, M., Dehaan, M., Pinto, H., Geerts, W. & Zinman, L. (2014) Venous thromboembolism in amyotrophic lateral sclerosis: a prospective study. *Neurology*, **82**, 1674–7.

Gonzalez-Covarrubias, V., Dane, A., Hankemeier, T. & Vreeken, R.J. (2013) The influence of citrate, EDTA, and heparin anticoagulants to human plasma LC–MS lipidomic profiling. *Metabolomics*, **9**, 337–348.

Guedes, A.F., Carvalho, F.A., Malho, I., Lousada, N., Sargento, L. & Santos, N.C. (2016) Atomic force microscopy as a tool to evaluate the risk of cardiovascular diseases in patients. *Nature nanotechnology*, **11**, 687–92.

Harris, F.M., Best, K.B. & Bell, J.D. (2002) Use of laurdan fluorescence intensity and polarization to distinguish between changes in membrane fluidity and phospholipid order. *Biochimica et biophysica acta*, **1565**, 123–8.

Jackson, S.P. (2011) Arterial thrombosis--insidious, unpredictable and deadly. *Nature medicine*, **17**, 1423–36.

JPK Instruments AG. (2012) *NanoWizard ® AFM Handbook*.

Kaibara, M. (1996) Rheology of blood coagulation. *Biorheology*, **33**, 101–17.

Karagkiozaki, V., Logothetidis, S., Laskarakis, a., Giannoglou, G. & Lousinian, S. (2008) AFM study of the thrombogenicity of carbon-based coatings for cardiovascular applications. *Materials Science and Engineering B: Solid-State Materials for Advanced Technology*, **152**, 16–21.

Kilinç, E., Rudež, G., Spronk, H.M.H., Nemmar, A., Maat, M.P.M. de, Cate, H. ten, *et al.* (2011) Particles, Coagulation, and Thrombosis. In *Cardiovascular Effects of Inhaled Ultrafine and Nanosized Particles*. John Wiley & Sons, Inc., Hoboken, USA, pp. 405–420.

Kim, H., Arakawa, H., Osada, T. & Ikai, A. (2003) Quantification of cell adhesion force with AFM: distribution of vitronectin receptors on a living MC3T3-E1 cell. *Ultramicroscopy*, **97**, 359–63.

Kim, J., Lee, H. & Shin, S. (2015) Advances in the measurement of red blood cell deformability: A brief review. *Journal of Cellular Biotechnology*, **1**, 63–79.

Kim, Y., Kim, K. & Park, Y. (2012) Measurement Techniques for Red Blood Cell Deformability: Recent Advances. In *Blood Cell - An Overview of Studies in Hematology*. InTech, pp. 167–194.

Kioumourtzoglou, M.-A., Rotem, R.S., Seals, R.M., Gredal, O., Hansen, J. & Weisskopf, M.G. (2015) Diabetes Mellitus, Obesity, and Diagnosis of Amyotrophic Lateral Sclerosis: A Population-Based Study. *JAMA neurology*, **72**, 905–11.

Kioumourtzoglou, M.-A., Seals, R.M., Gredal, O., Mittleman, M.A., Hansen, J. & Weisskopf, M.G. (2016) Cardiovascular disease and diagnosis of amyotrophic lateral sclerosis: A population based study. *Amyotrophic lateral sclerosis & frontotemporal degeneration*, **8421**, 1–7.

Kotzé, R.C.M., Ariëns, R.A.S., Lange, Z. de & Pieters, M. (2014) CVD risk factors are related to plasma fibrin clot properties independent of total and or γ' fibrinogen concentration. *Thrombosis research*, **134**, 963–9.

Lominadze, D. & Dean, W.L. (2002) Involvement of fibrinogen specific binding in erythrocyte aggregation. *FEBS letters*, **517**, 41–4.

Longo, D.L., Fauci, A.S. & Kasper, D.L. (2012) Disorders of the Cardiovascular System. In *Harrison's Principles of Internal Medicine*. pp. 1–7122.

Lovely, R.S., Kazmierczak, S.C., Massaro, J.M., D'Agostino, R.B., O'Donnell, C.J. & Farrell, D.H. (2010) γ' Fibrinogen: Evaluation of a New Assay for Study of Associations with Cardiovascular Disease. *Clinical Chemistry*, **56**, 781–788.

Ma, Y.-Q., Qin, J. & Plow, E.F. (2007) Platelet integrin alpha(IIb)beta(3): activation mechanisms. *Journal of thrombosis and haemostasis : JTH*, **5**, 1345–52.

Macrae, F.L., Domingues, M.M., Casini, A. & Ariëns, R.A.S. (2016) The (Patho)physiology of Fibrinogen γ'. *Seminars in thrombosis and hemostasis*, **42**, 344–55.

Mafuvadze, B. & Erlwanger, K.H. (2007) The effect of EDTA, heparin and storage on the erythrocyte osmotic fragility, plasma osmolality and haematocrit of adult ostriches (Struthio camelus). *Veterinarski Arhiv*, **77**, 427–434.

Malvern Instruments. (2004) *Zetasizer Nano Series - User Manual*. *Malvern Instruments MAN 0317*.

Malvern Instruments. (2011) Zeta potential: An Introduction in 30 minutes. In *Zetasizer Nano Series Technical Note. MRK654-01*. pp. 1–6.

Mannila, M.N., Lovely, R.S., Kazmierczak, S.C., Eriksson, P., Samnegård, A., Farrell, D.H., *et al.* (2007) Elevated plasma fibrinogen gamma' concentration is associated with myocardial infarction: effects of variation in fibrinogen genes and environmental factors. *Journal of thrombosis and haemostasis : JTH*, **5**, 766–73.

Martins e Silva, J. & Saldanha, C. (2005) Principais métodos de quantificação em Hemorreologia Clínica. *Boletim da SPHM*, **20**, 5–20.

Namazi, M.H., Khaheshi, I., Haybar, H. & Esmaeeli, S. (2014) Cardiac failure as an unusual presentation in a patient with history of amyotrophic lateral sclerosis. *Case reports in neurological medicine*, **2014**, 1–3.

Nanetti, L., Vignini, A., Raffaelli, F., Taffi, R., Silvestrini, M., Provinciali, L., *et al.* (2008) Sialic acid and sialidase activity in acute stroke. *Disease markers*, **25**, 167–73.

Neu, B., Wenby, R. & Meiselman, H.J. (2008) Effects of dextran molecular weight on red blood cell aggregation. *Biophysical journal*, **95**, 3059–65.

Parasassi, T., Krasnowska, E.K., Bagatolli, L. & Gratton, E. (1998) Laurdan and Prodan as Polarity-Sensitive Fluorescent Membrane Probes, **8**, 365–373.

Pronto-Laborinho, A.C., Pinto, S. & Carvalho, M. de. (2014) Roles of Vascular Endothelial Growth Factor in Amyotrophic Lateral Sclerosis. *BioMed Research International*, **2014**, 1–24.

Purves, D., Augustine, G.J., Fitzpatrick, D., Hall, W.C., Lamantia, A.-S., Mcnamara, J.O., *et al.* (2004) Neuroscience. In *Neuroscience*. pp. 1–773.

Rabai, M., Detterich, J.A., Wenby, R.B., Hernandez, T.M., Toth, K., Meiselman, H.J., *et al.* (2014) Deformability analysis of sickle blood using ektacytometry. *Biorheology*, **51**, 159–70.

Sachs, C., Conradi, S. & Kaijser, L. (1985) Autonomic function in amyotrophic lateral sclerosis: a study of cardiovascular responses. *Acta neurologica Scandinavica*, **71**, 373–8.

Saldanha, C. (2002) Mini review on erythrocyte aggregation - Basic Concepts and Clinical Repercussions. In *Boletim Hemorreologia n^{o}2 - Bolet-2*. pp. 1–10.

Sanchez, S.A., Tricerri, M.A. & Gratton, E. (2012) Laurdan generalized polarization fluctuations measures membrane packing micro-heterogeneity in vivo. *Proceedings of the National Academy of Sciences of the United States of America*, **109**, 7314–9.

Sanchez, S.A., Tricerri, M.A., Gunther, G. & Gratton, E. (2007) Laurdan Generalized Polarization: from cuvette to microscope. *Modern Research and Educational Topics in Microscopy*, **2**, 1007–1014.

Santos, M.J., Pedro, L.M., Canhão, H., Fernandes E Fernandes, J., Canas da Silva, J., Fonseca, J.E., *et al.* (2011) Hemorheological parameters are related to subclinical atherosclerosis in systemic lupus erythematosus and rheumatoid arthritis patients. *Atherosclerosis*, **219**, 821–6.

Sargento, L., Saldanha, C., Monteiro, J., Perdigão, C. & Martins e Silva, J. (2003) Evidence of prolonged disturbances in the haemostatic, hemorheologic and inflammatory profiles in transmural myocardial infarction survivors. *Thrombosis and haemostasis*, **89**, 892–903.

Shemisa, K., Kaelber, D., Parikh, S.A. & Mackall, J.A. (2014) Autonomic etiology of heart block in amyotrophic lateral sclerosis: a case report. *Journal of medical case reports*, **8**, 224.

Siemens Healthcare Diagnostics Products. (2008) Multifibren*U Fibrinogen.

Sociedade Portuguesa de Cardiologia. (2015) Prevenção Cardiovascular: Ideias e Números. *Revista Factores de Risco*, **36**, 1–58.

Springer, T.A., Zhu, J. & Xiao, T. (2008) Structural basis for distinctive recognition of fibrinogen γC peptide by the platelet integrin α IIb β 3. *The Journal of Cell Biology*, **182**, 791–800.

Stec, J.J., Silbershatz, H., Tofler, G.H., Matheney, T.H., Sutherland, P., Lipinska, I., *et al.* (2000) Association of fibrinogen with cardiovascular risk factors and cardiovascular disease in the Framingham Offspring Population. *Circulation*, **102**, 1634–8.

Stefanelli, V.L. & Barker, T.H. (2015) The evolution of fibrin-specific targeting strategies. *J. Mater. Chem. B*, **3**, 1177–1186.

Steffel, J., Lüscher, T.F. & Tanner, F.C. (2006) Tissue factor in cardiovascular diseases: molecular mechanisms and clinical implications. *Circulation*, **113**, 722–31.

Tanaka, Y., Yamada, M., Koumura, A., Sakurai, T., Hayashi, Y., Kimura, A., *et al.* (2013) Cardiac sympathetic function in the patients with amyotrophic lateral sclerosis: Analysis using cardiac [123I] MIBG scintigraphy. *Journal of Neurology*, **260**, 2380–2386.

Variola, F. (2015) Atomic force microscopy in biomaterials surface science. *Physical chemistry chemical physics : PCCP*, **17**, 2950–9.

Wagner, C., Steffen, P. & Svetina, S. (2013) Aggregation of Red Blood Cells: From Rouleaux to Clot Formation. *Comptes Rendus Physique*, **14**, 459–469.

Westerhof, N., Stergiopulos, N. & Noble, M. (2005) Snapshots of Hemodynamics: An aid for clinical research and graduate education. In *Snapshots of Hemodynamics: An aid for clinical research and graduate education*. pp. 1–3.

Wojcikiewicz, E.P., Zhang, X. & Moy, V.T. (2004) Force and Compliance Measurements on Living Cells Using Atomic Force Microscopy (AFM). *Biological procedures online*, **6**, 1–9.

Wolberg, A.S. (2016) Primed to Understand Fibrinogen in Cardiovascular Disease. *Arteriosclerosis, Thrombosis, and Vascular Biology*, **36**, 4–6.

World Health Organization. (2016) Cardiovascular diseases (CVDs) [WWW Document]. *World Health Organization (Fact sheet)*. URL http://www.who.int/mediacentre/factsheets/fs317/en/ [accessed on 2016].

World Health Organization. (2002) *The Atlas of Heart Disease and Stroke*. *Types of cardiovascular*, **1**, 18-19.

Xu, L.C. & Siedlecki, C. a. (2009) Atomic force microscopy studies of the initial interactions between fibrinogen and surfaces. *Langmuir*, **25**, 3675–3681.

Yu, M., Strohmeyer, N., Wang, J., Müller, D.J. & Helenius, J. (2015) Increasing throughput of AFM-based single cell adhesion measurements through multisubstrate surfaces. *Beilstein Journal of Nanotechnology*, **6**, 157–166.

Yu, W., So, P.T.C., French, T. & Gratton, E. (1996) Fluorescence Generalized Polarization of Cell Membranes : A Two-Photon Scanning Microscopy Approach. *Biophysical Journal*, **70**, 626–636.

Yurkin, M. a, Semyanov, K. a, Tarasov, P. a, Chernyshev, A. V, Hoekstra, A.G. & Maltsev, V.P. (2005) Experimental and theoretical study of light scattering by individual mature red blood cells by use of scanning flow cytometry and a discrete dipole approximation. *Applied optics*, **44**, 5249–5256.

Zhmurov, A., Brown, A.E.X., Litvinov, R.I., Dima, R.I., Weisel, J.W. & Barsegov, V. (2011) Mechanism of Fibrin(ogen) Forced Unfolding. *Structure*, **19**, 1615–1624.